



**RS2**

# **Thermal Analysis**

Verification Manual

# Table of Contents

<b>1. Steady State Heat Conduction</b> .....	<b>5</b>
1.1. Problem Description .....	5
1.2. Analytical Solution .....	7
1.2.1. Finite Element Method .....	7
1.2.2. Equation Method.....	8
1.3. Results .....	9
1.4. References.....	10
<b>2. Steady State Heated Strip</b> .....	<b>11</b>
2.1. Problem Description .....	11
2.2. Results .....	12
2.3. References.....	12
<b>3. Transient Heat Conduction</b> .....	<b>13</b>
3.1. Problem Description .....	13
3.2. Analytical Solution .....	13
3.3. Results .....	14
3.4. Reference.....	14
<b>4. Convective Surface on a Semi-infinite Domain</b> .....	<b>15</b>
4.1. Problem Description .....	15
4.2. Analytical Solution .....	16
4.3. Results .....	16
4.4. Reference.....	17
<b>5. Phase Change – Neumann’s Solution</b> .....	<b>18</b>
5.1. Problem Description .....	18
5.2. Analytical Solution .....	19
5.3. Results .....	19
5.4. Reference.....	20
<b>6. Phase Change – Freezing Analysis of a Buried Pipeline</b> .....	<b>21</b>
6.1. Problem Description .....	21
6.2. Model Geometry.....	21
6.3. Model Properties .....	21
6.4. Results .....	23
6.5. Reference.....	24

<b>7. Forced Convection with Water Transfer .....</b>	<b>25</b>
7.1. Problem Description .....	25
7.2. Analytical Solution .....	26
7.3. Results .....	27
7.4. Reference.....	27
<b>8. Phase Change – Water Transfer Forced Convection with Freezing .....</b>	<b>28</b>
8.1. Introduction.....	28
8.2. Problem description.....	28
8.3. Analytical Solution .....	30
8.4. Results .....	30
8.5. References.....	31
<b>9. Natural Convection .....</b>	<b>32</b>
9.1. Problem Description .....	32
9.2. Model Geometry.....	32
9.3. Model Properties .....	33
9.4. Results .....	34
9.5. References.....	37
<b>10.Surface Energy Balance.....</b>	<b>38</b>
10.1. Problem Description .....	38
10.2. Model Geometry.....	38
10.3. Material Properties .....	42
10.4. Results .....	44
10.5. Reference.....	44
<b>11.Thermal Conductivity – Cote and Konrad .....</b>	<b>45</b>
11.1. Introduction.....	45
11.2. Model Geometry.....	45
11.3. Material Properties .....	47
11.4. Results .....	47
11.5. Reference.....	48
<b>12.Thermal Conductivity Model – Johansen - Lu.....</b>	<b>49</b>
12.1. Problem Description .....	49
12.2. Material Properties .....	49
12.3. Results .....	50
12.4. References.....	51

<b>13. Thermosyphon – Laboratory Test</b> .....	<b>52</b>
13.1. Problem Description .....	52
13.2. Model Geometry.....	52
13.3. Material Properties .....	53
13.4. Results .....	55
13.5. References.....	56
<b>14. Thermosyphons in Pipeline Piles</b> .....	<b>57</b>
14.1. Problem Description .....	57
14.2. Model Properties .....	59
14.3. Results .....	63
14.4. References.....	67
<b>15. Thermal Expansion – 2D</b> .....	<b>68</b>
15.1. Problem Description .....	68
15.2. Analytical Solution .....	69
15.3. Results .....	69
<b>16. Thermal Expansion – 1D</b> .....	<b>71</b>
16.1. Problem Description .....	71
16.2. Analytical Solution .....	72
16.3. Results .....	72

# 1. Steady State Heat Conduction

## 1.1. Problem Description

This problem addresses calculation of temperature distribution in a two-dimensional square plate using linear triangular finite elements, adapted from Nithiarasu and Lewis (2012). Model 1 (Figure 1.1) uses a coarse mesh whilst model 2 uses an irregular fine mesh (Figure 1.2). A prescribed isothermal boundary condition of  $100^{\circ}\text{C}$  is set on all sides except the top, which is set as  $500^{\circ}\text{C}$ . The plate has a constant thermal conductivity of  $10\text{ W/m}^{\circ}\text{C}$ . The geometry of the problem is shown in Figure 1.1. The material properties used in the models are summarized in Table 1.1.

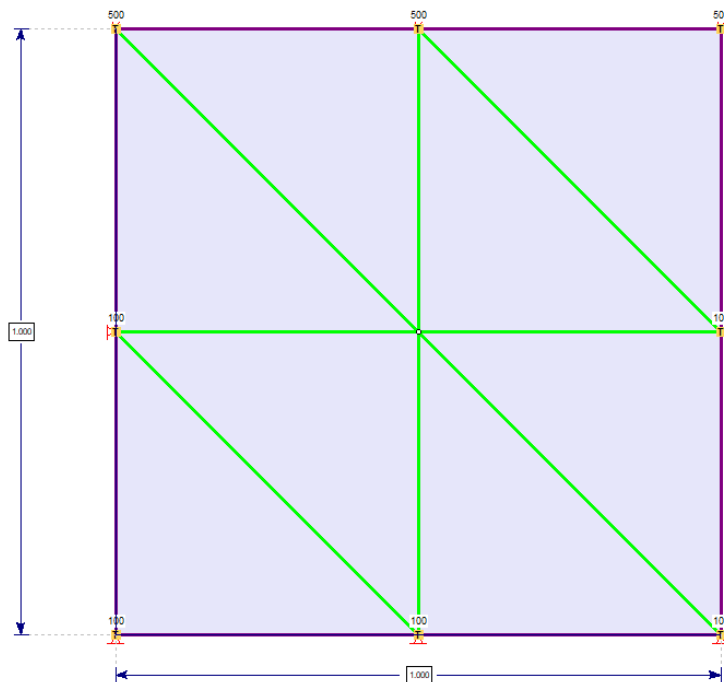


Figure 1.1: RS2 model 1 of a square plate

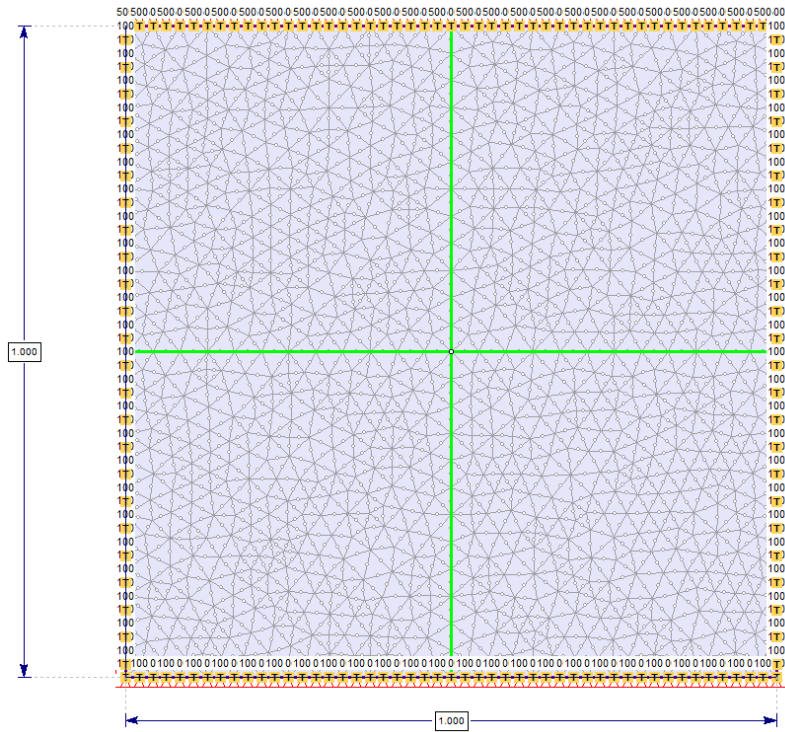


Figure 1.2: RS2 Model 2 of square plate

Table 1.1: Model parameters

Parameters	Value
<b>Thermal Properties</b>	
<b>Unfrozen Conductivity</b>	10
<b>Frozen conductivity</b>	10

## 1.2. Analytical Solution

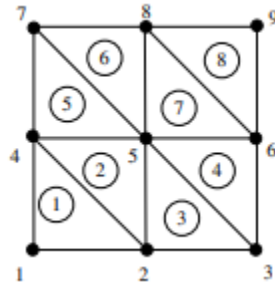


Figure 1.3: Triangular elements

### 1.2.1. Finite Element Method

Two sets of elemental  $[K]$  matrices exist because of the orientation of the triangles in Figure 1.3. For elements 1, 3, 5 and 7, the elements of the  $[K]$  matrix are:

$$\begin{aligned}
 b_1 &= y_2 - y_4; & c_1 &= x_4 - x_2 \\
 b_2 &= y_4 - y_1; & c_1 &= x_1 - x_4 \\
 b_4 &= y_1 - y_2; & c_4 &= x_2 - x_1
 \end{aligned}
 \tag{1.1}$$

The elemental  $[K]$  matrices:

$$[K]_1 = [K]_3 = [K]_5 = [K]_7 = \frac{tk}{4A} \begin{bmatrix} b_1^2 + c_1^2 & b_1b_2 + c_1c_2 & b_1b_4 + c_1c_4 \\ b_1b_2 + c_1c_2 & b_2^2 + c_2^2 & b_2b_4 + c_2c_4 \\ b_1b_4 + c_1c_4 & b_2b_4 + c_2c_4 & b_4^2 + c_4^2 \end{bmatrix}
 \tag{1.2}$$

Where  $b_1 = -0.5$ ,  $b_2 = 0.5$ ,  $b_4 = 0.5$ ,  $c_1 = -0.5$ ,  $c_2 = 0$ , and  $c_4 = 0.5$ .

The area of elements:

$$2A = \det \begin{bmatrix} 1.0 & 0.0 & 0.0 \\ 1.0 & 0.5 & 0.0 \\ 1.0 & 0.0 & 0.5 \end{bmatrix}
 \tag{1.3}$$

Where  $2A = 0.25m^2$ .

Final elemental equation:

$$[K]_1 = [K]_3 = [K]_5 = [K]_7 = \frac{tk}{2} \begin{bmatrix} 2.0 & -1.0 & -1.0 \\ -1.0 & 1.0 & 0.0 \\ -1.0 & 0.0 & 1.0 \end{bmatrix} \quad (1.4)$$

Similarly for elements 2, 4, 6 and 8, the elemental [K] matrices:

$$[K]_2 = [K]_4 = [K]_6 = [K]_8 = \frac{tk}{2} \begin{bmatrix} 1.0 & -1.0 & 0.0 \\ -1.0 & 2.0 & -1.0 \\ 0.0 & -1.0 & 1.0 \end{bmatrix} \quad (1.5)$$

The assembled equations:

$$\frac{tk}{2} \begin{bmatrix} 2.0 & -1.0 & 0.0 & -1.0 & 0.0 & 0.0 & 0.0 & 0.0 & 0.0 \\ -1.0 & 4.0 & -1.0 & 0.0 & -2.0 & 0.0 & 0.0 & 0.0 & 0.0 \\ 0.0 & -1.0 & 2.0 & 0.0 & 0.0 & -1.0 & 0.0 & 0.0 & 0.0 \\ -1.0 & 0.0 & 0.0 & 4.0 & -2.0 & 0.0 & -1.0 & 0.0 & 0.0 \\ 0.0 & -2.0 & 0.0 & -2.0 & 8.0 & -2.0 & 0.0 & -2.0 & 0.0 \\ 0.0 & 0.0 & -1.0 & 0.0 & -2.0 & 4.0 & 0.0 & 0.0 & -1.0 \\ 0.0 & 0.0 & 0.0 & -1.0 & 0.0 & 0.0 & 2.0 & -1.0 & 0.0 \\ 0.0 & 0.0 & 0.0 & 0.0 & -2.0 & 0.0 & -1.0 & 4.0 & -1.0 \\ 0.0 & 0.0 & 0.0 & 0.0 & 0.0 & -1.0 & 0.0 & -1.0 & 2.0 \end{bmatrix} \begin{bmatrix} T_1 \\ T_2 \\ T_3 \\ T_4 \\ T_5 \\ T_6 \\ T_7 \\ T_8 \\ T_9 \end{bmatrix} = \begin{bmatrix} 0.0 \\ 0.0 \\ 0.0 \\ 0.0 \\ 0.0 \\ 0.0 \\ 0.0 \\ 0.0 \\ 0.0 \end{bmatrix} \quad (1.6)$$

From equation ( 1.6 ) the only unknown  $T_5$  can be calculated from:

$$8T_5 = 2T_2 + 2T_4 + 2T_6 + 2T_8 \quad (1.7)$$

$$T_5 = 200 \text{ } ^\circ\text{C}.$$

### 1.2.2. Equation Method

$$T(x, y) = (T_{top} - T_{side}) \left( \frac{2}{\pi} \right) \sum_{n=1}^{\infty} \frac{(-1)^{n+1} + 1}{n} \sin\left(\frac{n\pi x}{w}\right) \frac{\sinh\left(\frac{n\pi y}{w}\right)}{\sinh\left(\frac{n\pi H}{w}\right)} + T_{side} \quad (1.8)$$

Where  $w$  is the width,  $H$  is the height of the plate,  $T_{top}$  is the temperature at the top boundary and  $T_{side}$  is the temperature on the other boundaries.

$$T(0.5, 0.5) = 200.11 \text{ } ^\circ\text{C}$$

### 1.3. Results

A query point plotted in RS2 at node 5 (0.5,0.5) on models 1 and 2 indicate  $T_5 = 200^\circ\text{C}$  which agrees with the analytical solutions presented. A fine meshed computer-generated analytical temperature contour was compared to that of RS2 model 2 (Figure 1.6) for further verification of temperature distribution throughout the square plate.

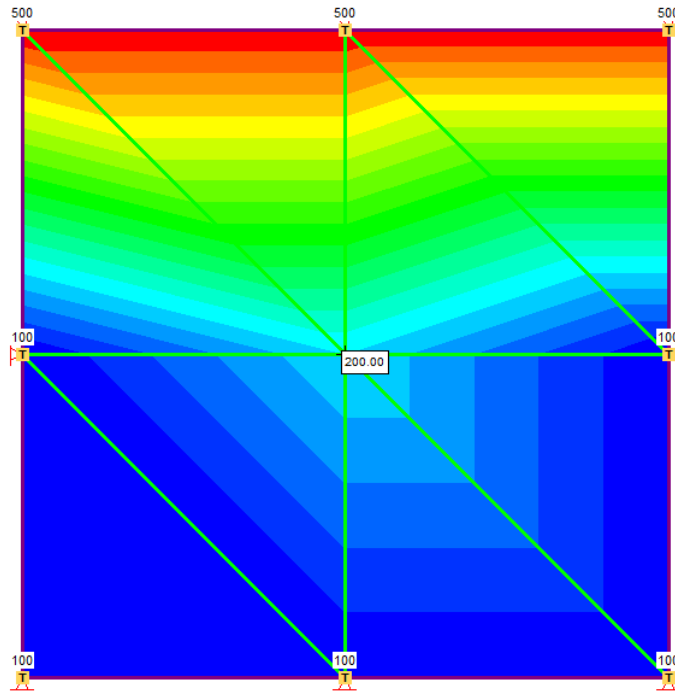


Figure 1.4: Model 1, coarse mesh solution

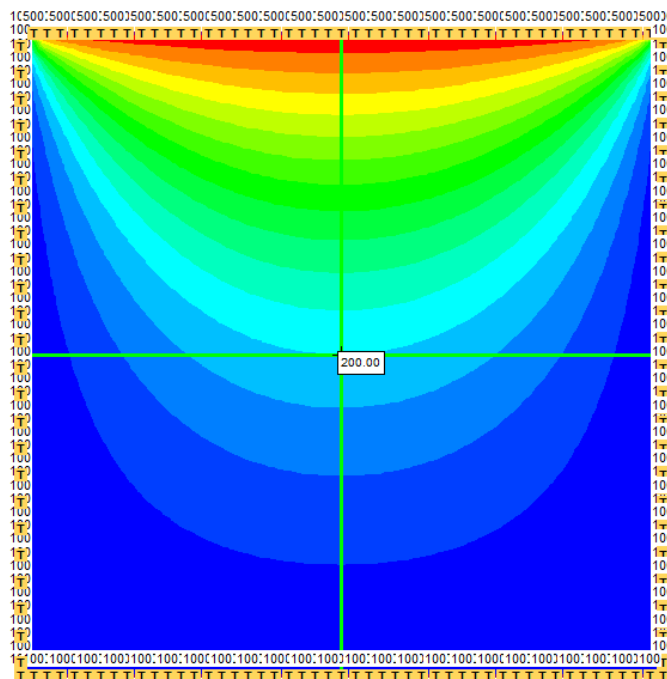


Figure 1.5: Model 2, fine mesh solution

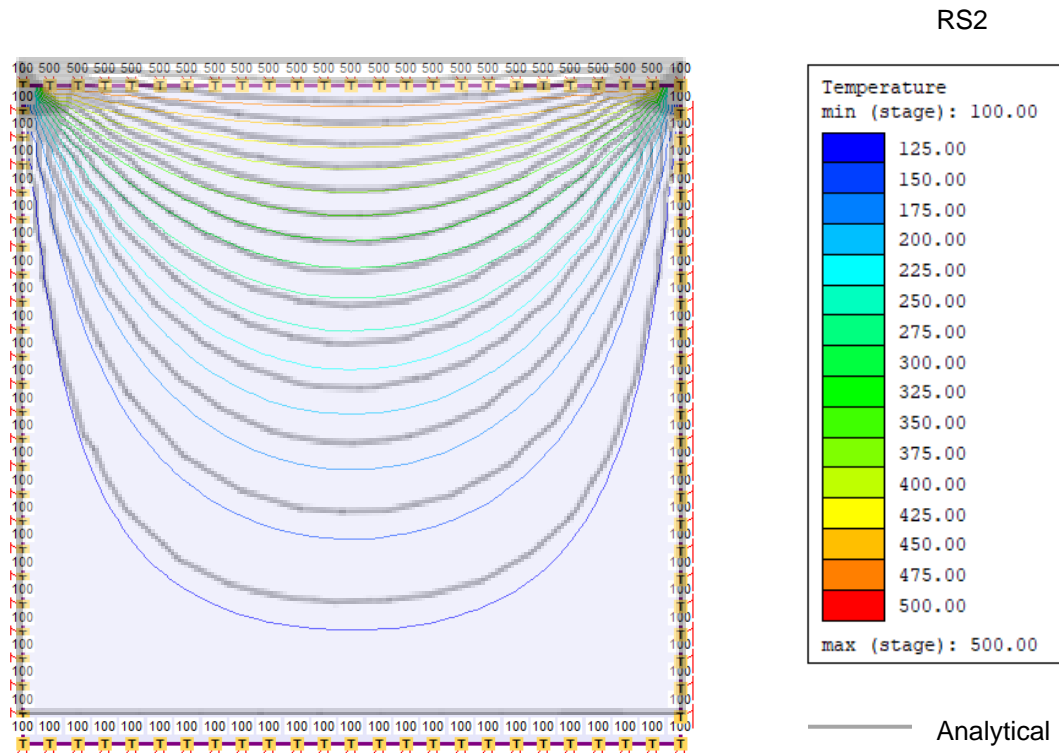


Figure 1.6: Analytical fine mesh temperature contour solution superimposed on RS2 fine mesh temperature contour solution. ( $T_{\min}=100^{\circ}\text{C}$ ,  $T_{\max}= 500^{\circ}\text{C}$  interval between two contours is  $25^{\circ}\text{C}$ )

## 1.4. References

Nithiarasu, P. and Lewis, R., 2012. Fundamentals of the finite element method for heat and fluid flow. Oxford: Wiley-Blackwell, pp.130-132: Example 5.2.1

# 2. Steady State Heated Strip

## 2.1. Problem Description

This problem addresses the effects of a heated strip extending across permafrost conditions. The results will be compared to that of TEMP/W software. The initial surface temperature of the model is  $-5^{\circ}\text{C}$  and increases with depth at a rate of  $1^{\circ}\text{C}/30\text{m}$ . A heated strip is then introduced at a constant temperature of  $4^{\circ}\text{C}$  extending across 50 m of the surface from (0,450) to (50,450). The geometry of the model can be seen in Figure 2.1. A random conductivity of  $1\text{ W/m/C}$  was used. A uniform fine 6 noded triangle mesh was used to ensure convergence and solution accuracy.

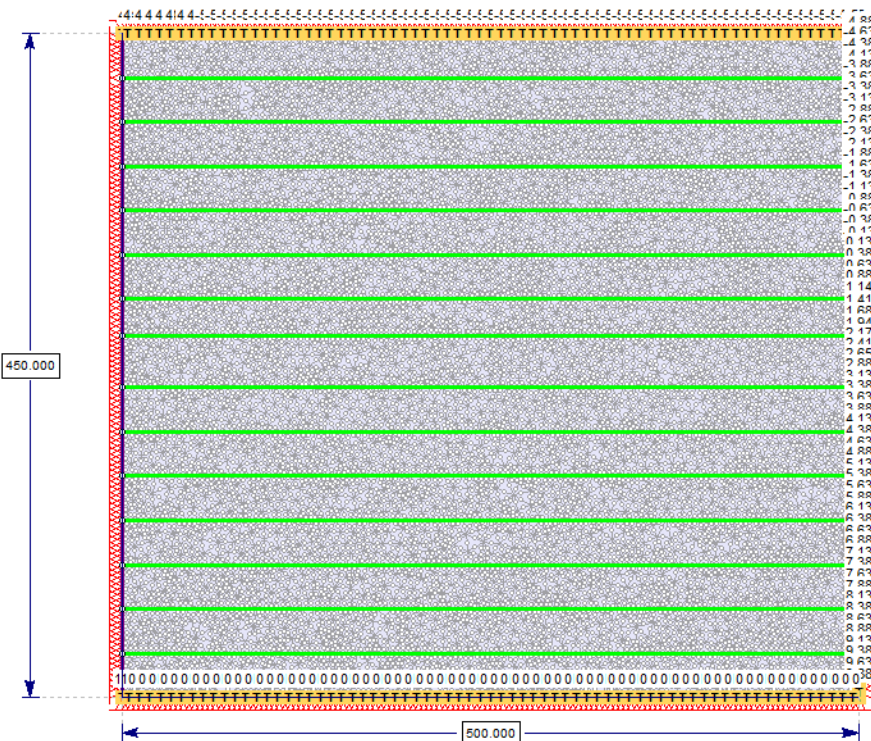


Figure 2.1: Model geometry

## 2.2. Results

Figure 2.2 shows good agreement between the RS2 result and TEMP/W verified solution.

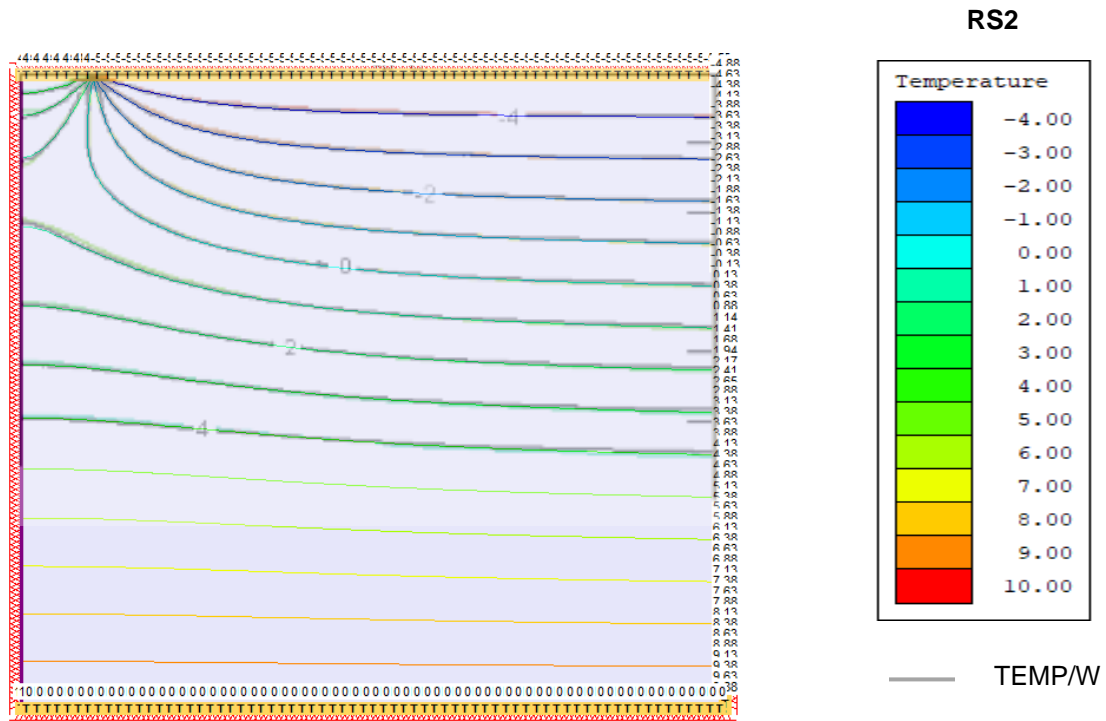


Figure 2.2: RS2 results versus TEMP/W verified solution

## 2.3. References

GEO-SLOPE International Ltd. Temp/W example models. Heated Strip.

# 3. Transient Heat Conduction

## 3.1. Problem Description

This problem adapted from Nithiarasu and Lewis (2012) through a rod of 1m width and 20m length. The initial temperature of the rod is 0°C. A heat flux of 1 W/m is introduced on the left boundary and all other sides are insulated as seen in Figure 3.1. The material properties used are summarized in Table 3.1. Since both conductivity and heat capacity are constants and no latent heat was considered, the unfrozen water content curve information is not needed.

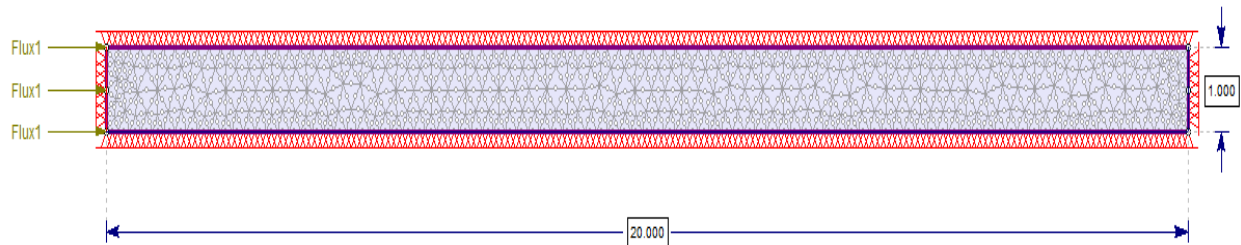


Figure 3.1: RS2 model

Table 3.1: Model Properties

Parameters	Value
<b>Initial Conditions</b>	
Unit weight	9.81 kN/m <sup>3</sup>
<b>Thermal Properties</b>	
Conductivity type	Constant
Unfrozen Conductivity (W/m/C)	1
Frozen conductivity (W/m/C)	1
Thermal volumetric heat capacity type	Constant
Unfrozen volumetric heat capacity (J/m3/C)	1
Frozen volumetric heat capacity (J/m3/C)	1

## 3.2. Analytical Solution

Calculation of Temperature through the rod is given by:

$$T(x, t) = 2 \left( \frac{t}{\pi} \right)^{1/2} \left[ \exp \left( -\frac{x^2}{4t} \right) - \left( \frac{1}{2} \right) x \sqrt{\frac{\pi}{t}} \operatorname{erfc} \left( \frac{x}{2\sqrt{t}} \right) \right] \quad (3.1)$$

### 3.3. Results

Figure 3.2 shows the temperature variation along the length of the rod in RS2 in comparison to the temperature calculated using the analytical solution. The results indicate strong agreement with the analytical solution.

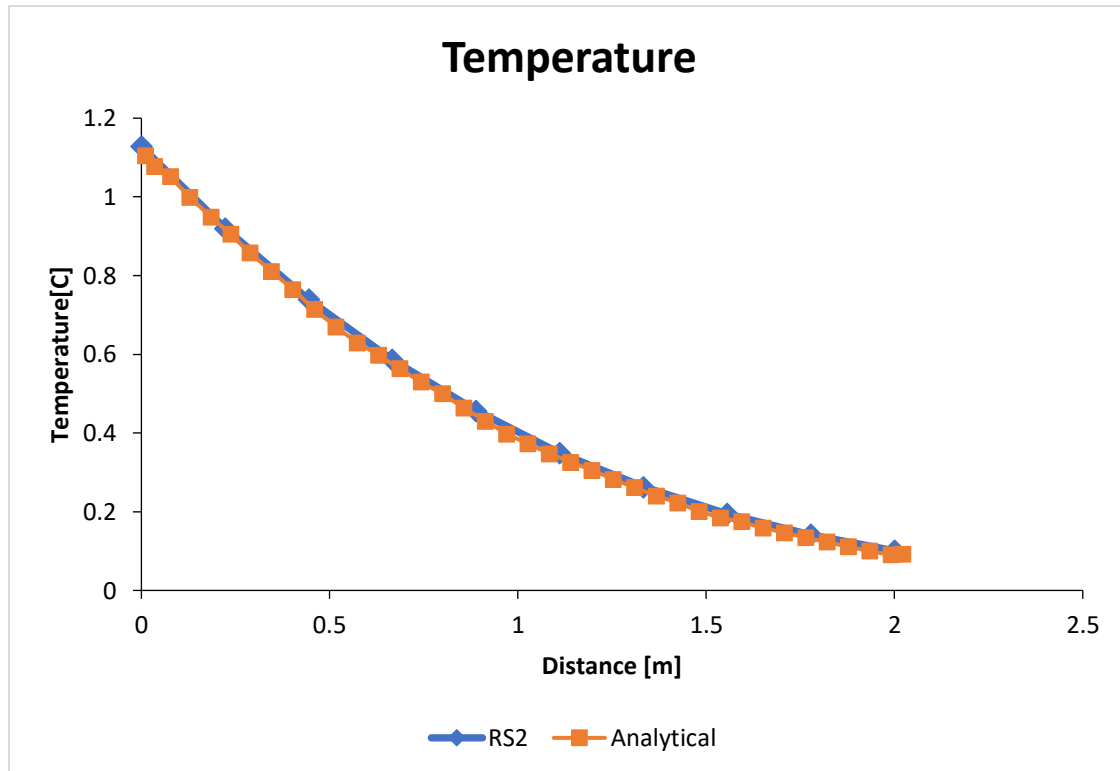


Figure 3.2: Temperature distribution along the rod at t=1

### 3.4. Reference

Nithiarasu, P. and Lewis, R., (2012). Fundamentals of the finite element method for heat and fluid flow. Oxford: Wiley-Blackwell, pp.159-160: Example 6.4.2.

## 4. Convective Surface on a Semi-infinite Domain

---

### 4.1. Problem Description

This problem attempts to validate the RS2 implementation of convection boundary conditions which allows users to simulate energy transfer by diffusion from a bounding surface into a moving fluid. This model features a 10m column with an initial temperature of 20°C. The lower boundary is kept at a constant temperature of 20°C and assumed far enough from the bounding surface to characterize the domain as semi-infinite. The surface of the column is subjected to changes in conditions simulating fluid flowing over the surface at a constant temperature of -15°C for a duration of 1 day (86,400 seconds). The convective heat transfer coefficient is assumed constant at 40 J/s/m<sup>2</sup>/ °C. The geometry of the problem can be seen in Figure 4.1 and the properties used in the model are summarized in Table 4.1.

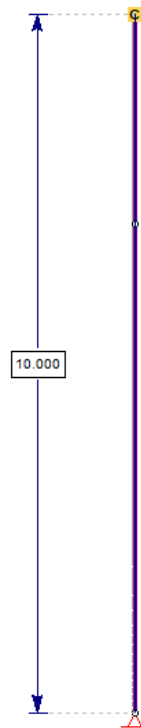


Figure 4.1: RS2 model of the problem statement

Table 4.1: Model Properties

Parameters	Value
<b>Initial Conditions</b>	
<b>Unit weight (kN/m<sup>3</sup>)</b>	1E-06 kN/m <sup>3</sup>
<b>Porosity</b>	0.999999
<b>Thermal Properties</b>	
<b>Water content value (m<sup>3</sup>/m<sup>3</sup>)</b>	0.999999
<b>Unfrozen Conductivity (W/m/°C)</b>	0.52
<b>Frozen conductivity (W/m/°C)</b>	0.52
<b>Thermal heat capacity type</b>	Constant
<b>Use latent heat</b>	No
<b>Unfrozen volumetric heat capacity (J/m<sup>3</sup>/°C)</b>	3.772E+06
<b>Frozen volumetric heat capacity (J/m<sup>3</sup>/°C)</b>	3.772E+06
<b>Thermal soil unfrozen water content type</b>	Simple

## 4.2. Analytical Solution

An analytical solution is provided by Carslaw and Jaeger (1986).

## 4.3. Results

Figure 4.2 shows the temperature variation at the bounding surface as time increase. The results show the RS2 solution agrees with that of the analytical solution.

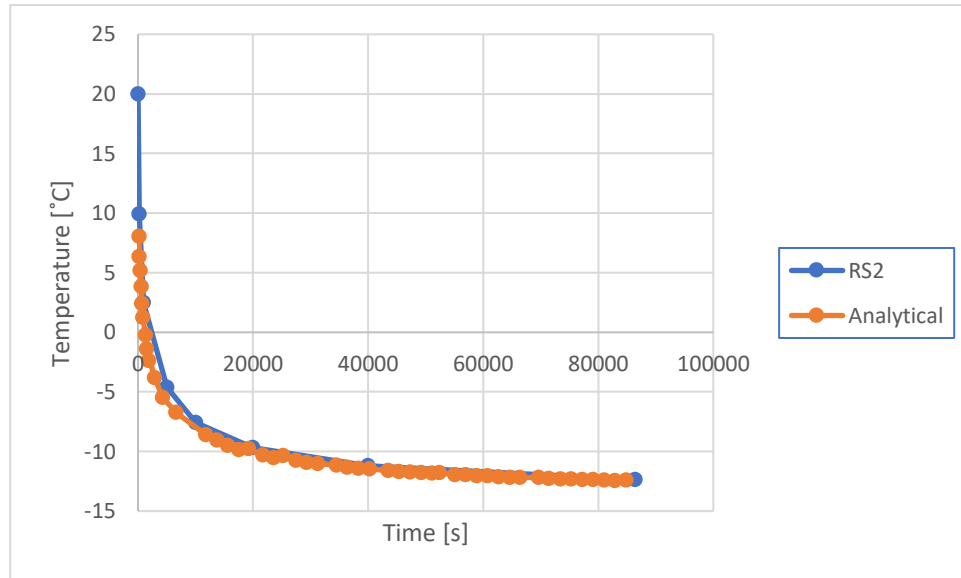


Figure 4.2: Temperature vs Time at the top of the semi-infinite domain.

#### 4.4. Reference

Carslaw, H.S. and Jaeger, J.C. (1986). Conduction of heat in solids. *Oxford Science Publication, 2nd Edition*.

## 5. Phase Change – Neumann’s Solution

---

### 5.1. Problem Description

This problem attempts to validate the RS2 implementation of Neumann’s solution, a numerical analysis of phase change problems. A phase change problem involves the release or absorption of thermal energy in the region undergoing the change of state. In this case, the process of thawing (absorption of energy) will be addressed. The model comprises of a 10m column with an initial temperature of  $-2^{\circ}\text{C}$ . The domain is a semi-infinite region where the lower boundary is kept at the initial temperature of  $-2^{\circ}\text{C}$  and the upper boundary is set to  $2^{\circ}\text{C}$  to activate thawing. The duration of the analysis is taken over 100 days. It should be noted a simplified thermal model was used where complete phase change occurs at  $0^{\circ}\text{C}$ . The geometry of the problem can be seen in Figure 5.1 and the properties used in the model are summarized in Table 5.1. The soil column has a porosity of 0.99999 to represent pure water. The unfrozen water content curve has a very steep slope with the fully solidus temperature at  $-0.001$  Celsius degrees. Normally, when dealing with phase change simulation with steep unfrozen water content curve, other programs will have to use small time step to capture the phase change accurately. RS2 uses an advance enthalpy compensation algorithm so that the simulation does not need to use very small time step to capture the phase change with soils that has very steep unfrozen water content curve.

Table 5.1: Model properties

Parameters	Value
Water content value	0.999
Unfrozen Conductivity (kW/m/C)	0.0015
Frozen conductivity (kW/m/C)	0.0015
Thermal volumetric heat capacity type	Jame Newman
Include latent heat	Yes
Soil specific heat capacity (kJ/tons/C)	755
Thermal soil unfrozen water content type	Custom

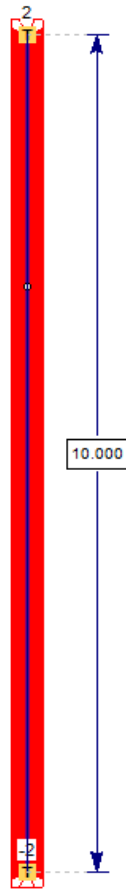


Figure 5.1: RS2 model of problem statement

## 5.2. Analytical Solution

An analytical solution was found by Neumann in the 1860s and is provided by Carslaw and Jaeger (1986).

## 5.3. Results

Figure 5.2 represents the temperature variation profile along the column calculated in RS2 and Neumann's solution for 10, 50 and 100 days. The figure shows RS2 results in great agreement with that of Neumann's thus validate the ability of RS2 to model phase change behaviours effectively. Note that RS2 use average of 3 time steps per stage and still capture the frozen front as well as the temperature distribution correctly.

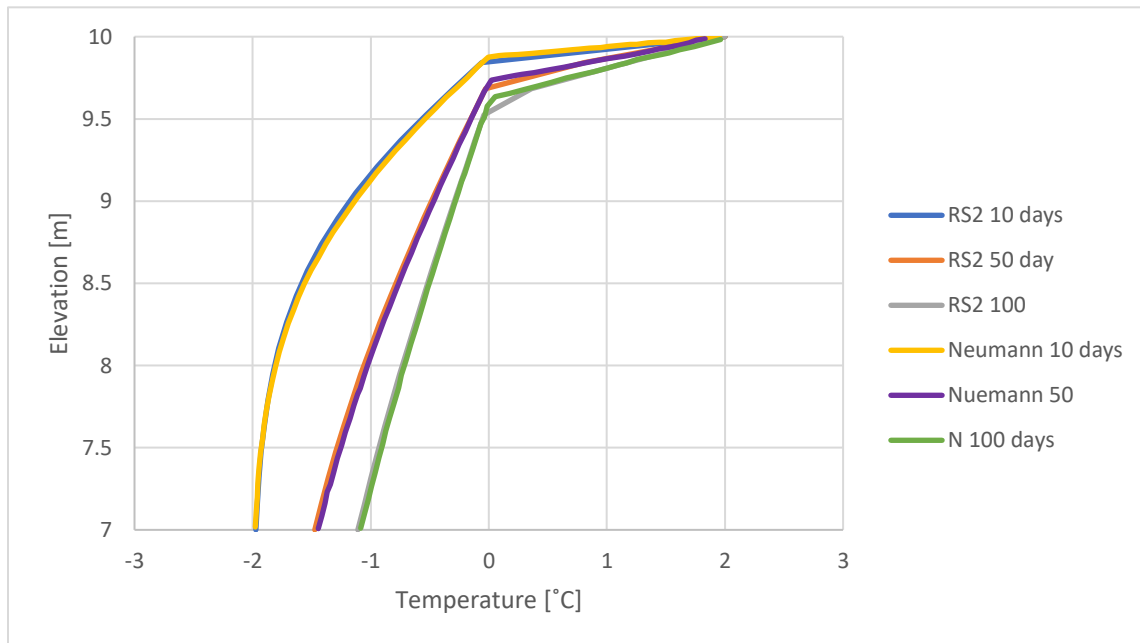


Figure 5.2: Comparison of solutions

## 5.4. Reference

Carslaw, H.S. and Jaeger, J.C. (1986). Conduction of heat in solids. *Oxford Science Publication, 2nd Edition*.

# 6. Phase Change – Freezing Analysis of a Buried Pipeline

## 6.1. Problem Description

This problem addresses the use of RS2 to model the changing thermal profile around a buried pipeline. Verification of RS2 results will be compared against results published by Coutts and Konrad (1994).

## 6.2. Model Geometry

The model comprises of 1.6m by 3.2m area of soil as seen in Figure 6.1. The centre of the pipe is located at the middle of the domain at 1.6m and elevation of 1.15m, with a radius of 0.15m. The initial temperature condition of the domain is 3°C. The temperature of the pipe is set to -2°C after initial condition is established. The analysis is taken over a period of 730 days (6.3072e+07 s). 20 stages were used with initial increments of 1 day and increasing exponentially.

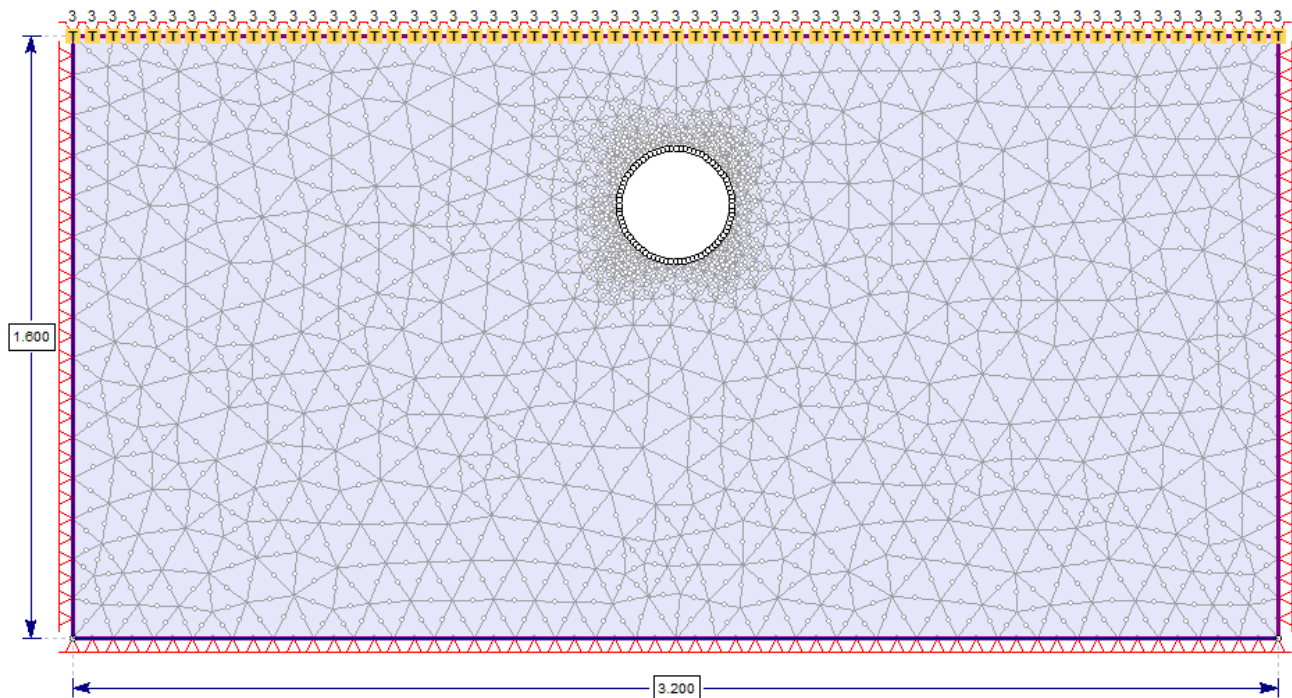


Figure 6.1: RS2 model geometry

## 6.3. Model Properties

The material properties of the soil used in the model can be found in Table 6.1. Custom thermal conductivity and thermal soil unfrozen water content functions were used, as seen in Figure 6.2 and Figure 6.3 respectively.

Table 6.1: Material properties

Parameters	Value
<b>Thermal Properties</b>	
Water content (m <sup>3</sup> /m <sup>3</sup> )	0.3772
Thermal Conductivity method	Custom
Dependency	Temperature
Thermal volumetric heat capacity type	Constant
Include latent heat	Yes
Unfrozen heat capacity (kJ/m <sup>3</sup> /°C)	1950
Frozen heat capacity (kJ/m <sup>3</sup> /°C)	1950
Frozen temperature (°C)	0
Thermal soil unfrozen water content type	Custom

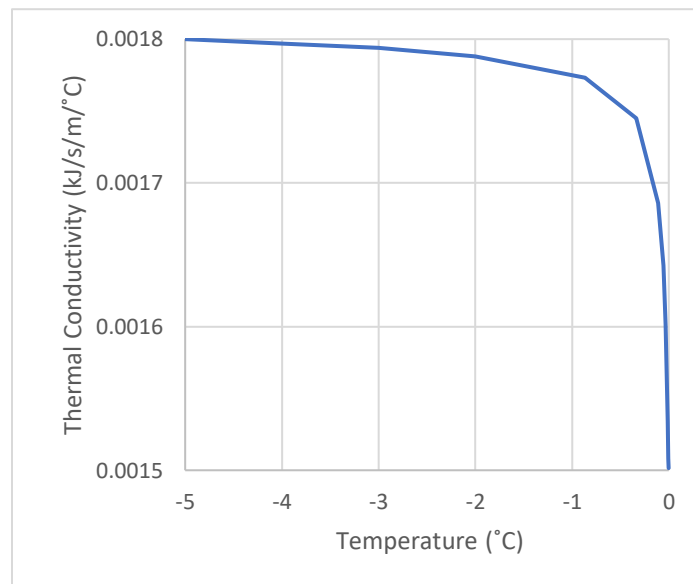


Figure 6.2: Thermal conductivity function

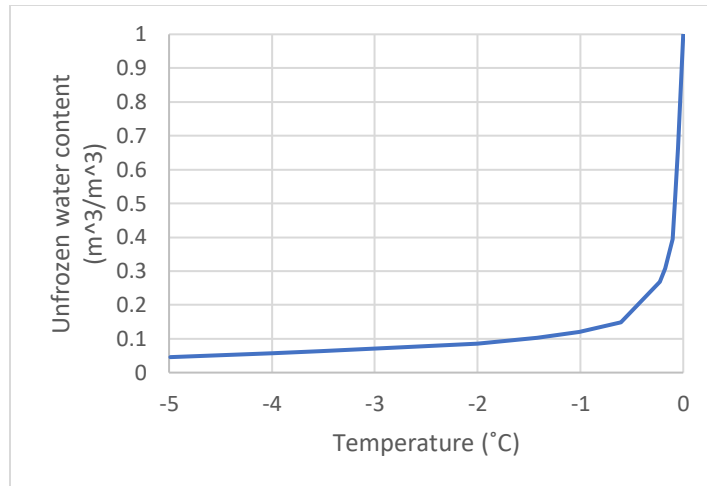


Figure 6.3: Unfrozen water content function

## 6.4. Results

Coutts and Konrad (1994) studied the extent of freezing around a pipe using “Node State” finite element method. They computed that after two years the freezing front would be approximately 0.6m and 0.23m, below and beside the pipeline, respectively. The RS2 thermal contour result after the two year simulation period is shown in comparison to that published by Coutts and Konrad (1994), as seen in Figure 6.4. RS2 estimates the freezing front to be 0.6m below the pipe, in good agreement with Coutts and Konrad (1994) estimations. The RS2 freezing front width is approximately 0.23m beside the pipe, this is also consistent with Coutts and Konrad (1994).

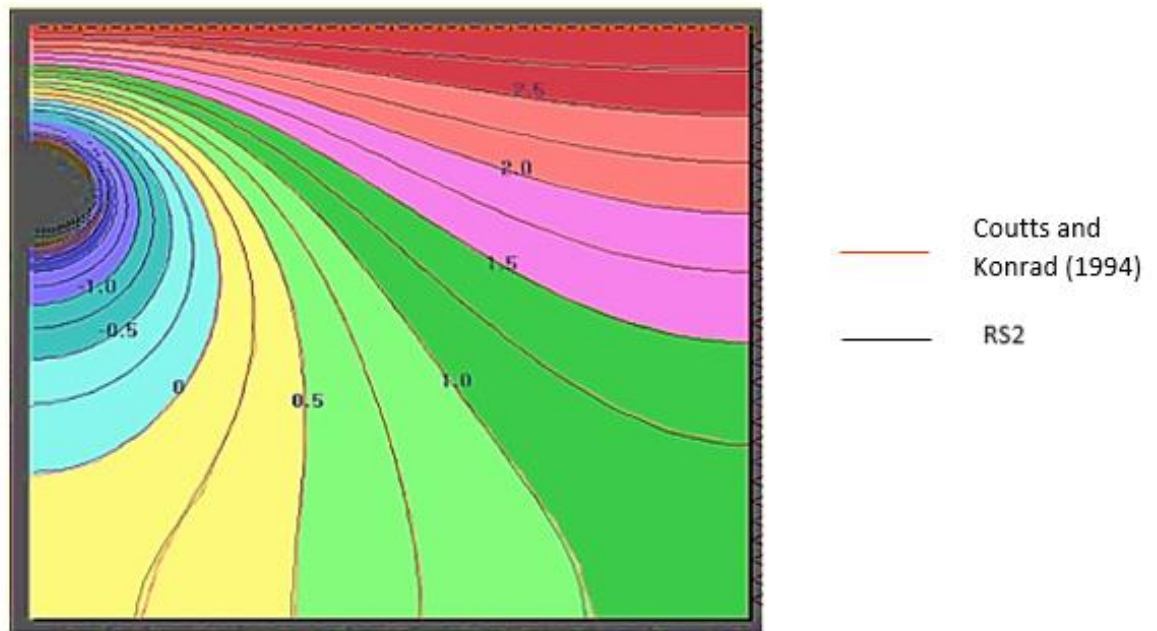


Figure 6.4: Temperature contours on day 730 Coutts and Konrad (1994) and RS2.

Figure 6.5 shows the changing positions of the freezing front with time RS2.

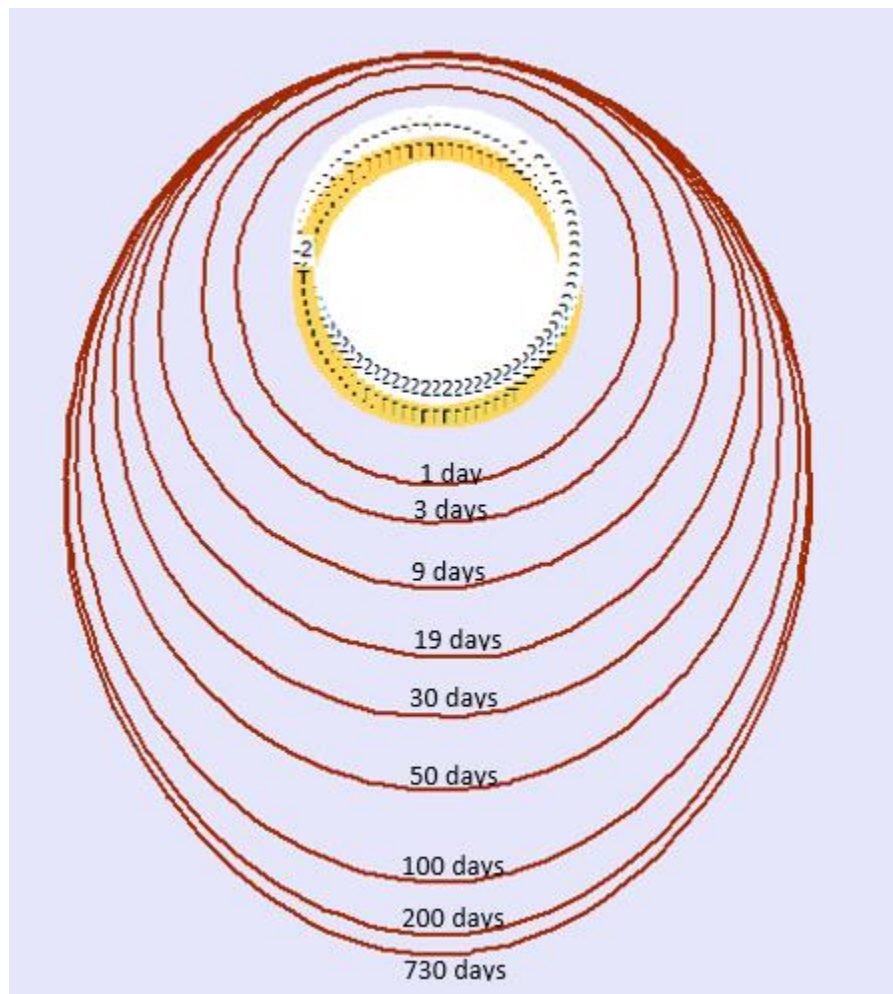


Figure 6.5: Isolines of changing freezing front with time.

## 6.5. Reference

Coutts, R.J. and Konrad, J.M. (1994). Finite element modeling of transient non-linear heat flow using the node state method. *International Ground Freezing Conference, France*.

# 7. Forced Convection with Water Transfer

---

## 7.1. Problem Description

This case aims to verify RS2 ability to model force by which heat transfer occurs with a flowing fluid. In this case, the heat advection will be produced by flowing water condition. The model comprises of a column of length 0.3m with an initial temperature of 0°C. The temperature of the bottom remains at 0°C while the temperature of the top is set to 1°C, creating a downward conduction heat gradient. The hydraulic boundary conditions were defined to create a steady-state flux of  $q_w = 3.33e-8$  m/s. The top hydraulic boundary is 0.31 and the bottom is 0.3 to create a downward gradient. The boundary conditions are reversed to create and upward gradient. The duration of the analysis is taken over 150 days (1.296e+07 seconds) until a steady state was achieved. Figure 7.1 shows the geometry of the case.

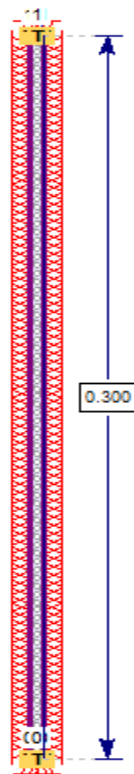


Figure 7.1: Problem statement geometry

Three different cases were considered in:

Model 1-The hydraulic and thermal gradients are in the same downward gradient direction.

Model 2- The thermal gradient is downward and the hydraulic gradient is upwards (opposite directions).

Model 3- The Hydraulic and thermal gradients are normal so that the streamlines for fluid flow are collinear with the isotherms of heat conduction (i.e. fluid flow is from left to right).

Force convection option is activated for Model 2 and 3. The model properties listed are listed in Table 7.1.

Table 7.1: Model properties

Parameters	Value
<b>Hydraulic properties</b>	
Material behaviour	Drained
Ks (m/s)	1e-06
K2/K1	1
K1 angle (degrees)	0
WC curve slope (m3/m3/kPa)	1e-05
mv (m3/m3/kPa)	1e-05
<b>Thermal Properties</b>	
Water content (m3/m3)	Use from Groundwater
Thermal Conductivity method	Constant
Unfrozen Conductivity (W/m/C)	0.01
Frozen conductivity (W/m/C)	0.01
Frozen temperature (C)	0
Thermal heat capacity type	constant
Include latent heat	no
Unfrozen volumetric heat capacity (J/m3/C)	2.5e+06
Frozen volumetric heat capacity (J/m3/C)	2.5e+06
Thermal soil unfrozen water content type	Simple

## 7.2. Analytical Solution

The partial differential equation for one-dimensional steady-state heat transfer by conduction and advection with flowing water is given by:

$$\frac{d^2T}{dy^2} = \frac{\rho_w c_w q_w}{k} \frac{dT}{dy} = 0 \quad (7.1)$$

Where  $\rho_w$  is water density,  $c_w$  is mass specific heat,  $q_w$  is water flux and  $k$  is the thermal conductivity. The solution to equation ( 7.1 ) (Bredehoeft and Papadopoulos, 1965) is given by:

$$T_y = T_o + \frac{[T_L - T_o] \left[ \exp \left( N_{PE} \frac{y}{L} \right) - 1 \right]}{[\exp(N_{PE}) - 1]} \quad (7.2)$$

Where  $T_L$  and  $T_o$  are the temperature at the top and bottom of the porous unit,  $L$  is the thickness and  $N_{PE}$  is the Peclet number for heat transfer given by:

$$N_{PE} = \frac{\rho_w c_w q_w L}{K} \quad (7.3)$$

Assuming  $\rho_w = 1000 \text{ kg/m}^3$  and  $c_w = 4186 \text{ J/kg/K}$

$$N_{PE} = 4.186$$

### 7.3. Results

The temperature profiles for all models against the analytical solution presented is seen in Figure 7.2. Each RS2 solution shows great agreement with that of the analytical solution. The forced convection produces great alteration of the conductive temperature profile in models 1 and 2. Whilst for model 3, there is no effects of forced convection due to the streamlines for fluid flow being colinear with the isotherms of heat conduction.

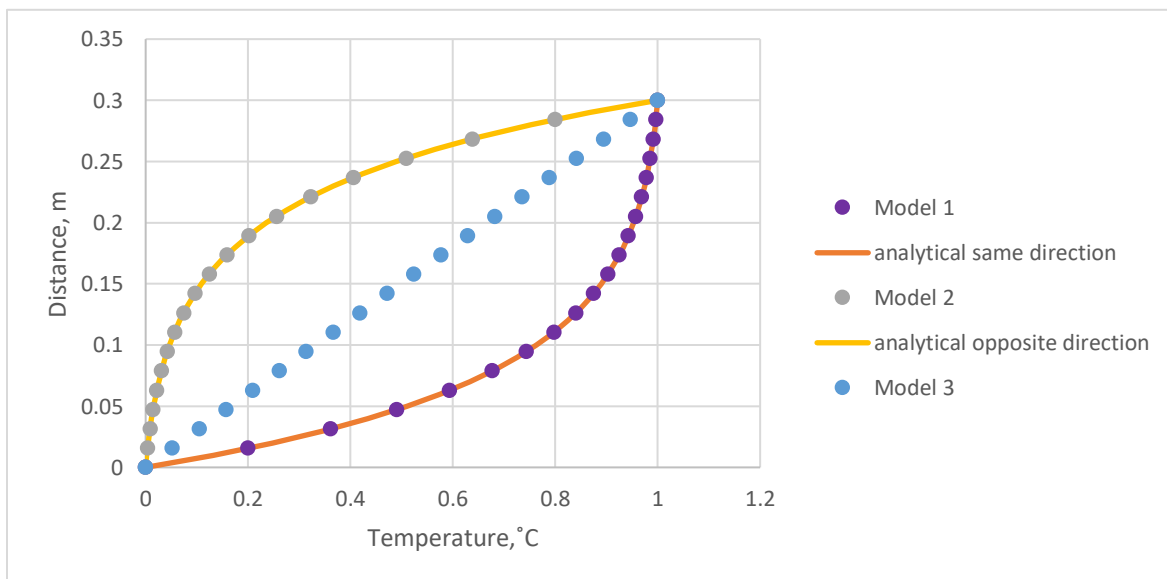


Figure 7.2: Temperature profile along the column

### 7.4. Reference

Bredehoeft, J. and Papadopulos, I.S. (1965). Rates of vertical groundwater movement estimated from the earth's thermal profile. *Water Resources Res.* 1: 325-328.

# 8. Phase Change – Water Transfer Forced Convection with Freezing

## 8.1. Introduction

RS2 has previously been verified against the Neumann closed form equation for phase change problems and heat transfer by conduction. Also, RS2 was verified against an analytical solution for heat transfer by conduction and forced convection with flowing water in the absence of phase change. This problem further attempts to validate the forementioned verifications by including phase change in the analysis of heat transfer by conduction and forced convection by water transfer. Forces convection option in project setting was activated for this verification.

## 8.2. Problem description

The problem is a forced convection analysis based on conditions described by Kurylyk et al. (2014). The model comprises of a column of 10m length with an initial temperature of  $-1e-03$  °C. The lower boundary is kept at the initial temperature and the upper is set to 1 °C to activate thawing. The constant head boundary conditions of 11m and 1m were set to the upper and lower boundary, respectively. This ensured the column remained saturated and simulated the saturated hydraulic conductivity to reflect the Darcy velocity of 100m/year. The analysis is taken over a 20 days period. Figure 8.1 shows the geometry of model. The material properties used in the analysis can be found in Table 8.1. Unfrozen water content curve is shown in Figure 8.2.

Table 8.1: Material properties

Parameters	Value
<b>Hydraulic properties</b>	
Material behaviour	Drained
Ks (m/s)	3.17e-06
K2/K1	1
K1 angle (degrees)	0
WC curve slope (m3/m3/kPa)	1e-05
Mv (m3/m3/kPa)	1e-05
<b>Thermal Properties</b>	
Water content (m3/m3)	0.5
Thermal conductivity method	Constant
Unfrozen conductivity (W/m/C)	1.839
Frozen conductivity (W/m/C)	2.649
Frozen temperature (C)	0

<b>Thermal volumetric heat capacity type</b>	Constant
<b>Include latent heat</b>	Yes
<b>Unfrozen heat capacity (J/m3/C)</b>	3.201e+06
<b>Frozen heat capacity (J/m3/C)</b>	2.163e+06
<b>Thermal soil unfrozen water content type</b>	Custom

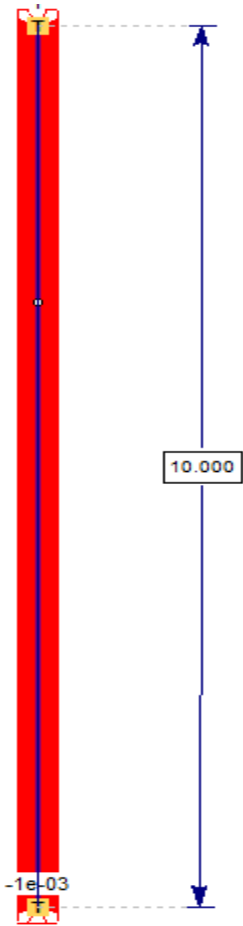


Figure 8.1: RS2 model 2

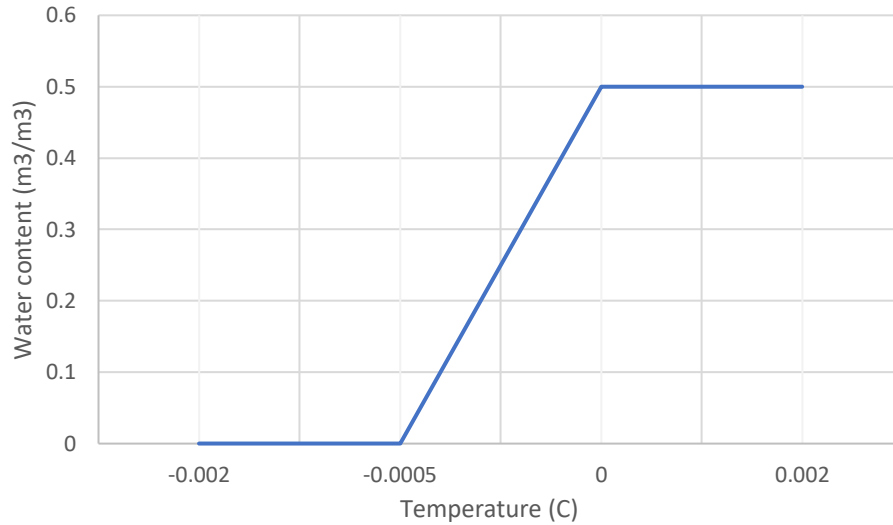


Figure 8.2: Unfrozen water content curve

### 8.3. Analytical Solution

The location of the thaw front ( $X$ ) developed by Lunardini (1998):

$$X + \frac{\alpha}{v_t} \left\{ \exp\left(\frac{v_t X}{\alpha}\right) - 1 \right\} = v_t S_T t \quad (8.1)$$

Where  $\alpha$  is the thermal diffusivity of the unfrozen zone,  $v_t$  is the velocity of the thermal plume without conduction,  $S_T$  is the Stefan number, and  $t$  is the time.

The assumption that the thawing front is moving gradually enough to be considered under steady-state conditions, allows for the use of the steady-state conduction- advection equation:

$$\alpha \frac{d^2 T}{dx^2} - v_t \frac{dT}{dx} = 0 \quad (8.2)$$

### 8.4. Results

Figure 8.3 shows comparison between the Lunardini's solution and RS2. The thaw front location for the duration of the analysis is compared. The figure shows RS2 is in good agreement with Lunardini's solution. Again, the enthalpy compensation algorithm in RS2 shown excellent performance when the similar results from Kurylyk et al. can only be obtained using very small time step.

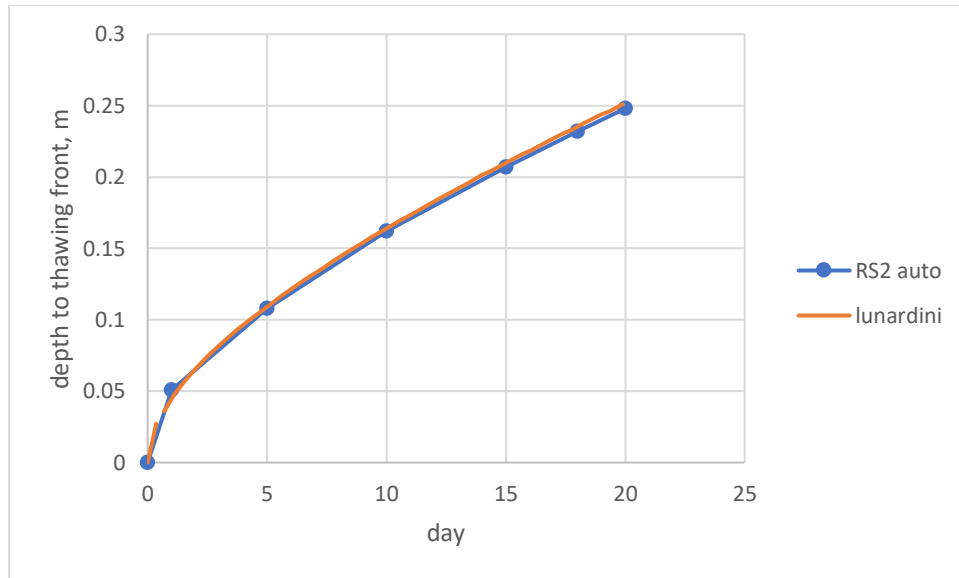


Figure 8.3: Location of thaw front over 20 days period

## 8.5. References

Kurylyk, B.L., McKenzie, J.M., MacQuarrie, K.T.B., and Voss, C.I. (2014). Analytical solutions for benchmarking cold regions subsurface water flow and energy transport models: one-dimensional soil thaw with conduction and advection. *Advances in Water Resources* 70: 172-184.

Lunardini, V.J. (1998). Effect of convective heat transfer on thawing of frozen soil. In: Lewkowicz, A.G., Allard, M. (ed). Proceedings of the seventh international conference on permafrost. *Yellowknife, Canada*: 689-695.

# 9. Natural Convection

## 9.1. Problem Description

Groundwater flow plays an important role in thermal dissipation and can be driven by topography and buoyancy. Topography driven flow occurs due to differences in elevation of water table which creates difference in potential energy driving fluid from high elevation to low elevation, often referred to as forced convection. Buoyancy-driven flow results from variations in fluid density associated with changes in temperature. This is usually referred to as free or natural convection. This example demonstrates RS2 modelling of the groundwater flow conditions mentioned above and will be compared to the numerical simulation conducted by Yang, Feng, Luo and Chen, (2010). In order to include the natural convection behaviors, Natural Convection and Force Convection options are activated in project setting.

## 9.2. Model Geometry

Two transient hydro-thermal analysis will be conducted.

Model 1:

This model will simulate natural convection. The domain is 200m in height and has a width of 800m. There is no change in topography, the surface is flat. The temperature of the top and bottom boundary is kept at 20°C and 26°C, respectively. The top surface is assigned a groundwater boundary condition of zero pressure (Figure 9.1). Natural convection and forced convection are toggled on in thermal project settings and a TIN triangulation grid interpolation is used. The analysis is taken over 206 years (6.49642e+09 secs), with the stage increases starting with 1-year steps. After 26 years the steps increase to 5 years.

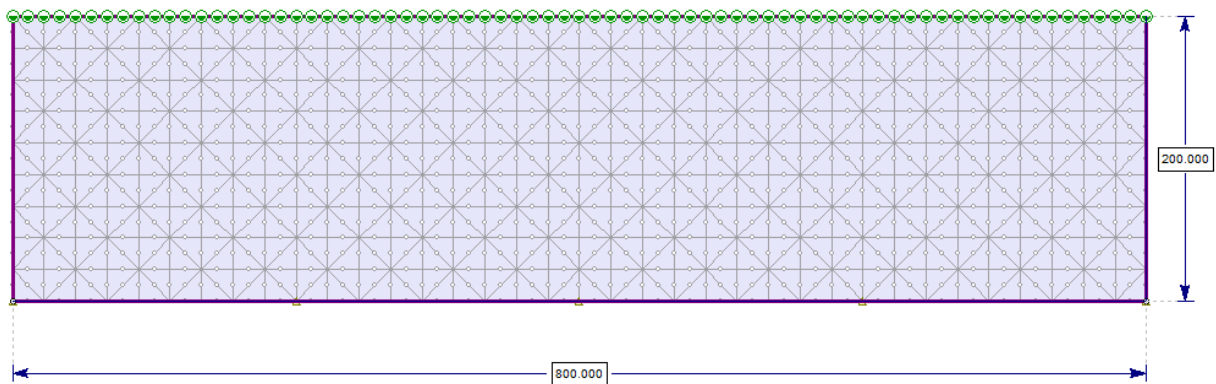


Figure 9.1: Model 1 geometry

Model 2:

This model will simulate both natural and forced convection. There is a slight alteration in the geometry from model 1. The top surface sloped with a difference in height of 20 cm. All other conditions in the model 1 remain the same. The analysis is taken over 5e04 days (4.32e+09secs), with the stage increases starting with 1year steps. After 26 years the steps increase to 5 years.

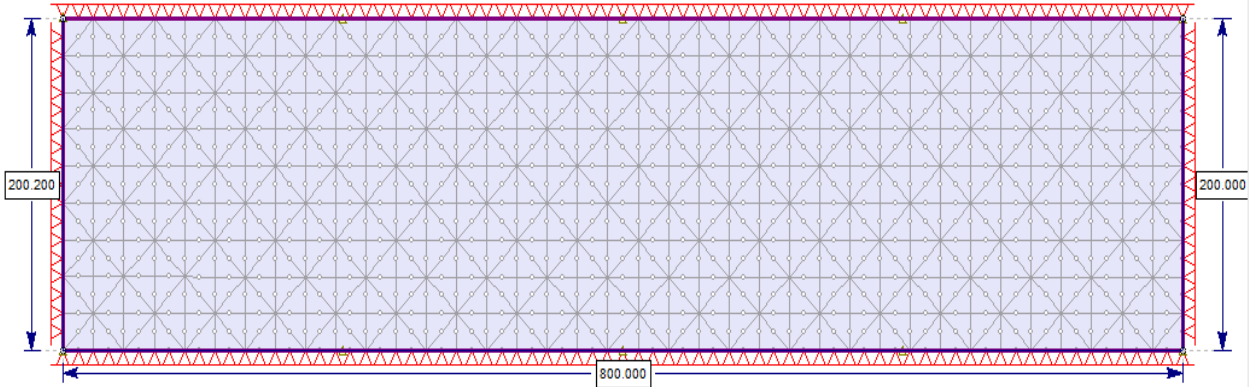


Figure 9.2: Model 2 geometry

### 9.3. Model Properties

The hydraulic and thermal properties used in each model are the same and seen in Table 9.1.

Table 9.1: Material properties

Parameter	Value
Unit weight (kN/m <sup>3</sup> )	23.22
Porosity	0.1
<b>Hydraulic properties</b>	
Model	Constant
Material behaviour	Drained
Ks (m/s)	0.00012
K2/K1	1
K1 definition	Angle
Angle (degrees)	0
WC curve slope (m <sup>3</sup> /m <sup>3</sup> /kPa)	1e-06
Use mv	Yes

<b>Mv (m3/m3/kPa)</b>	1e-06
<b>Thermal properties</b>	
<b>Water content value (m3/m3)</b>	0.1
<b>Thermal conductivity method</b>	Constant
<b>Unfrozen conductivity (kW/m/C)</b>	0.00218
<b>Frozen conductivity (kW/m/C)</b>	0.00218
<b>Thermal volumetric heat capacity</b>	Constant
<b>Unfrozen heat capacity (kJ/m<sup>3</sup>/C)</b>	2311
<b>Frozen heat capacity (kJ/m<sup>3</sup>/C)</b>	2311
<b>Thermal soil unfrozen water content</b>	Simple
<b>Thermal expansion</b>	No
<b>Dispersivity</b>	No

## 9.4. Results

The RS2 results are compared to the results of a similar simulation conducted by Yang, Feng, Luo and Chen, (2010). It should be noted that the Yang, Feng, Luo and Chen, (2010) simulation does not use the same material properties as RS2 example as there are some typos in the paper leading to contradicted values. Thus, the model parameters were chosen so that similar results were obtained. Since the slope is 0, there was no existing groundwater flow in the model at the beginning. Model 1 groundwater flow is only affected by natural convection (Figure 9.3 and Figure 9.4). As the slope increases to 0.00025, Model 2 experiences the effects of both forced convection and natural convection (Figure 9.5 and Figure 9.6).

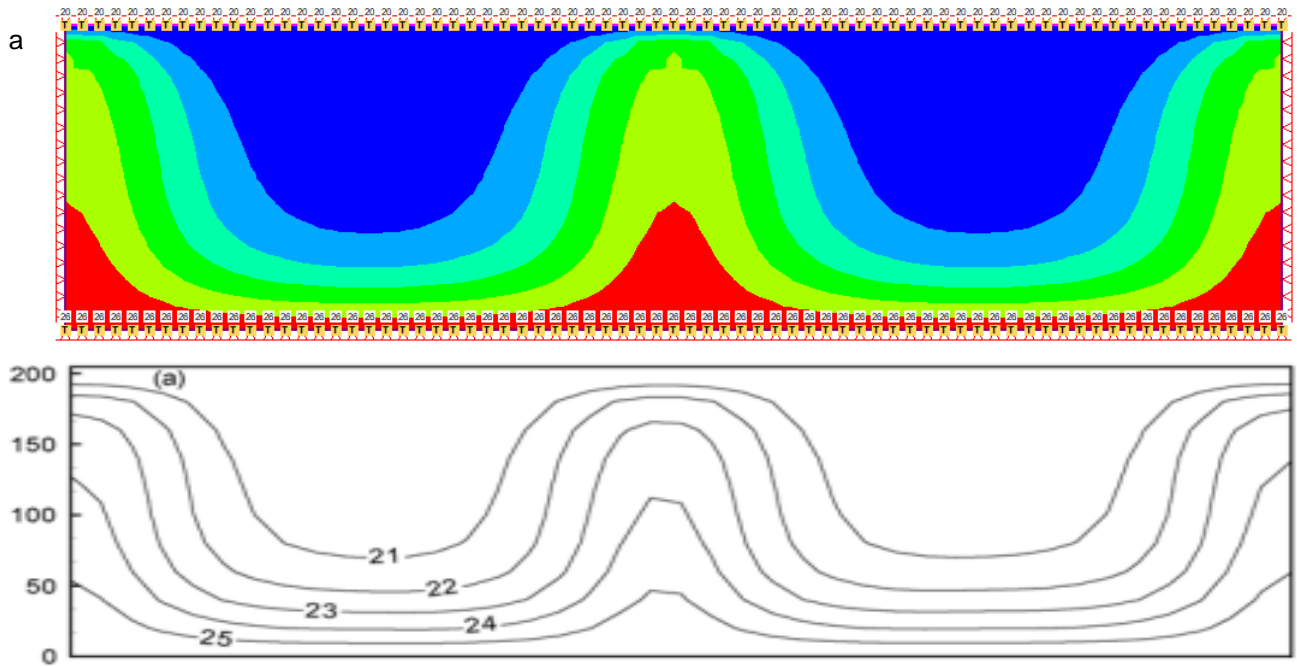


Figure 9.3: Model 1 temperature contours. a) RS2 at time =206 years, b) Yang, Feng, Luo and Chen, (2010) at steady state

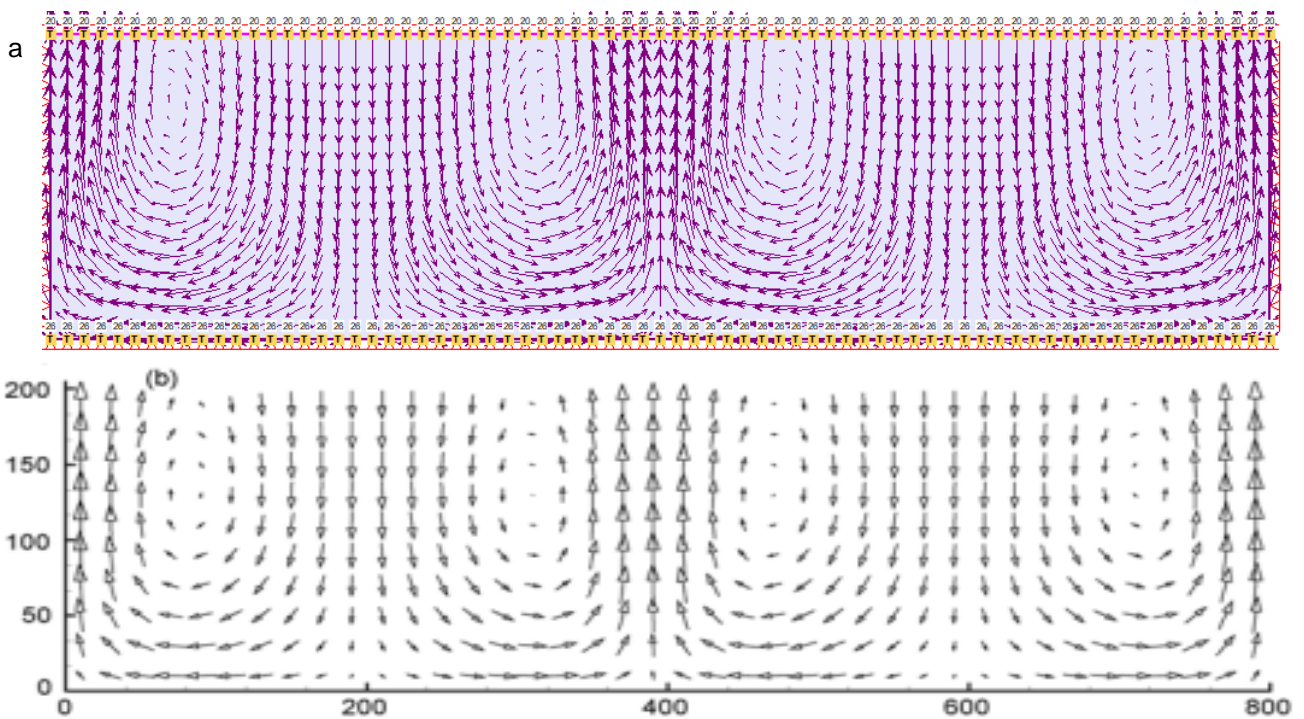


Figure 9.4: Model 1 flow vectors. A) RS2 at time =206 years, b) Yang, Feng, Luo and Chen, (2010) at steady state

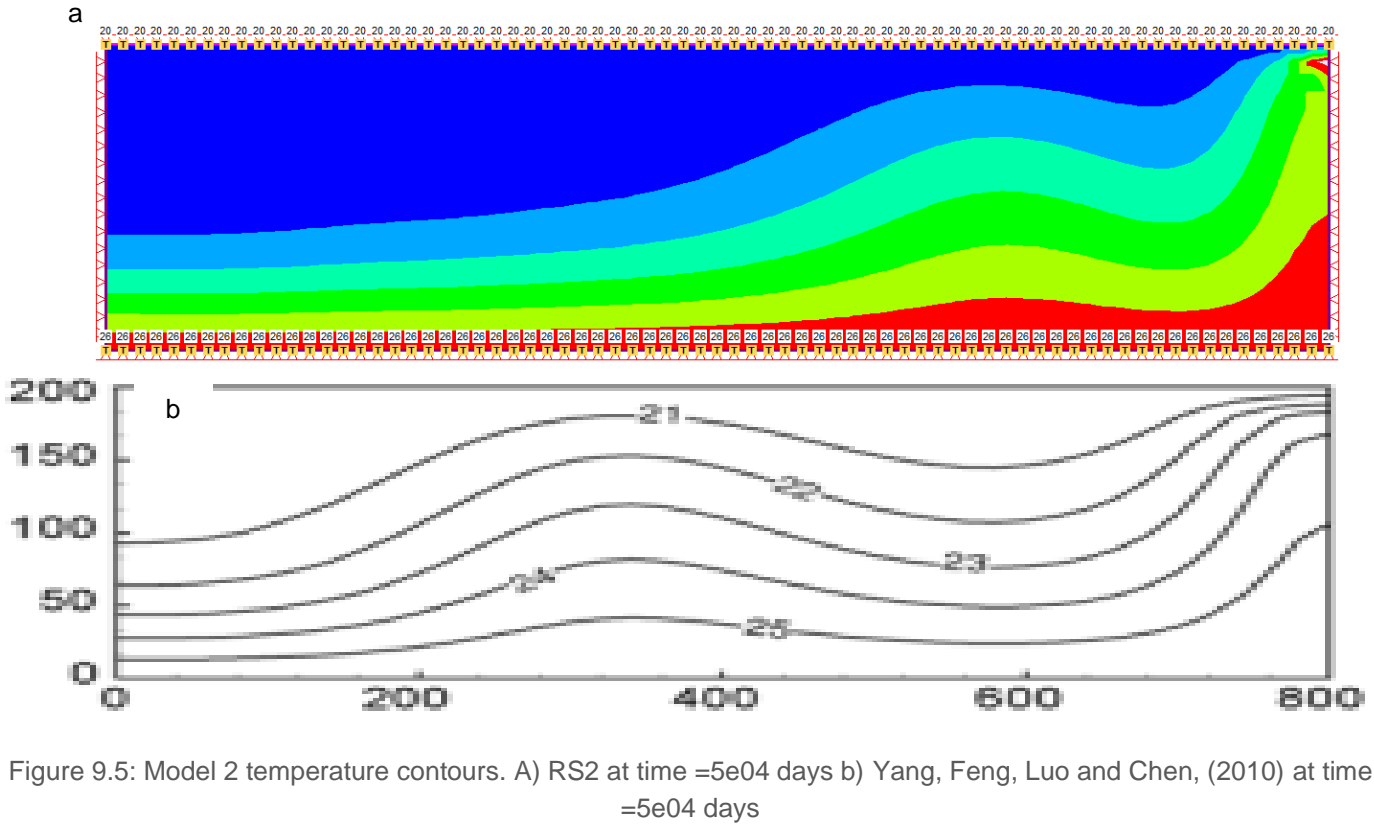


Figure 9.5: Model 2 temperature contours. A) RS2 at time =5e04 days b) Yang, Feng, Luo and Chen, (2010) at time =5e04 days

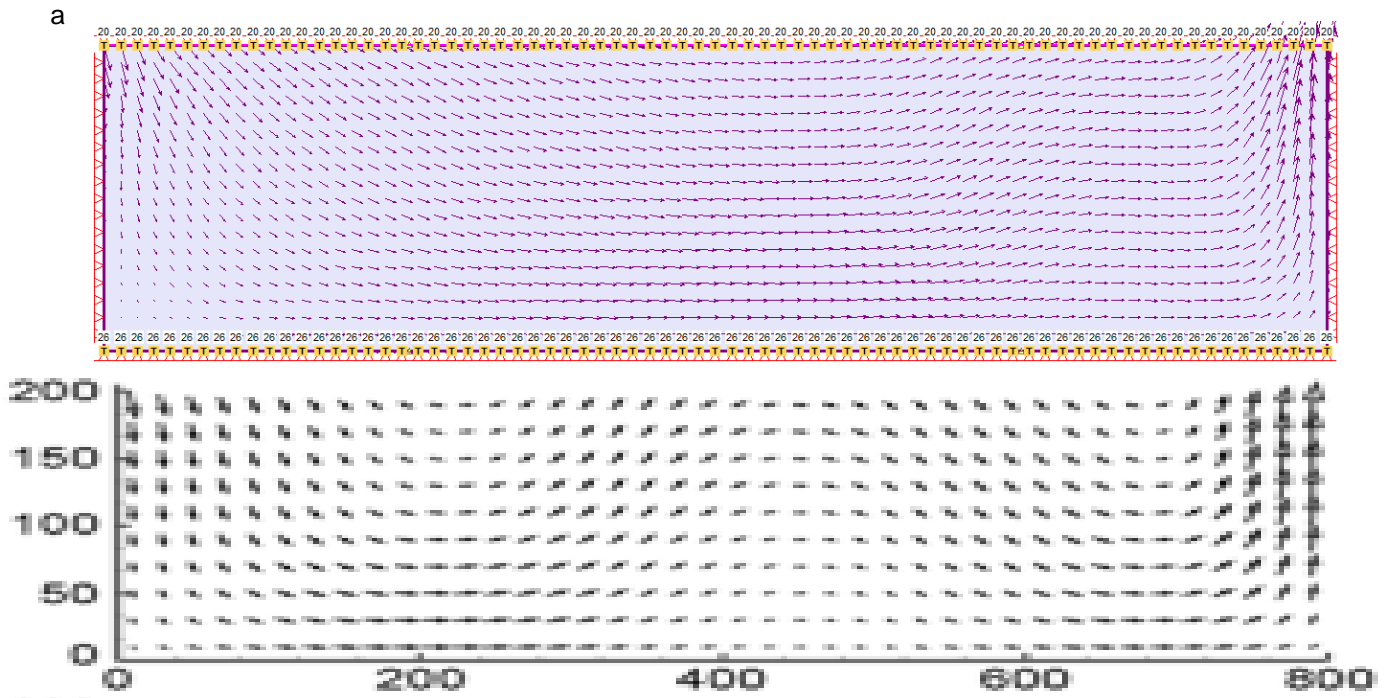


Figure 9.6: Model 2 flow vectors. A) RS2 at time =5e04 days, b) Yang, Feng, Luo and Chen, (2010) at 5e04 days

## 9.5. References

Yang, J., Feng, Z., Luo, X. and Chen, Y.(2010). Numerically quantifying the relative importance of topography and buoyancy in driving groundwater flow. *Science in China Series D: Earth Sciences*, 53(1), pp.64-71.

# 10. Surface Energy Balance

## 10.1. Problem Description

This problem addresses RS2 implementation of a surface energy balance boundary considering climatic data. The model will simulate the behaviour of a warm gas pipeline on permafrost. The modelled predictions of Hwang (1976) and measured field data collected by the Canadian Artic Gas Study Limited will be used to verify RS2 results.

## 10.2. Model Geometry

The model comprises of a 30.15 m column of soil with a thermal grid defining initial temperature conditions. The ground surface is assigned as a heat transfer section. At the bottom boundary there is a constant flux of  $8e-05$  kW/m. At the top boundary the flux is time dependent with respect to meteorological data. The geometry of the model is seen in Figure 10.1. The analysis is taken over 360 days ( $3.1104e+07$  s) with stages set from day 0, day 1 (86400 s), day 10 (864000 s) and 10 day increments continuing, for a total of 37 stages.

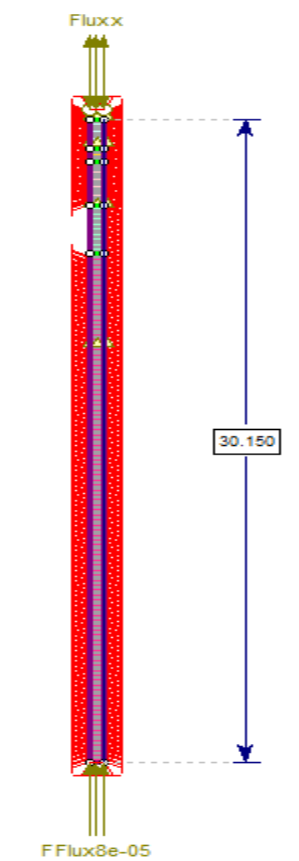


Figure 10.1: RS2 model geometry

The model inputs are as follows:

Table 10.1: RS2 temperature grid

X coordinate (m)	Y coordinate (m)	Temperature (°C)
0.6	62.0573	7.77778
0.6	60.8381	0
0.6	57.9425	-2.22222
0.6	51.3893	-2.22222
0.6	0	-2.22222
0.0001	62.0573	7.77778
0.0001	60.8381	0
0.0001	57.9425	-2.22222
0.0001	51.3893	-2.22222
0.0001	0	-2.22222
0.3	62.0573	7.77778
0.3	60.8381	0
0.3	57.9425	-2.22222
0.3	51.3893	-2.22222
0.3	0	-2.22222

Top boundary Flux Climate Conditions:

Table 10.2: Top boundary flux climate conditions

Type	Data
Start time	0 s
Total time	427 days
Radiation	Calculate from Solar Radiation
Define Vegetation	yes
Define snow pack	yes
Snow conductivity (kW/m/C)	0.0001

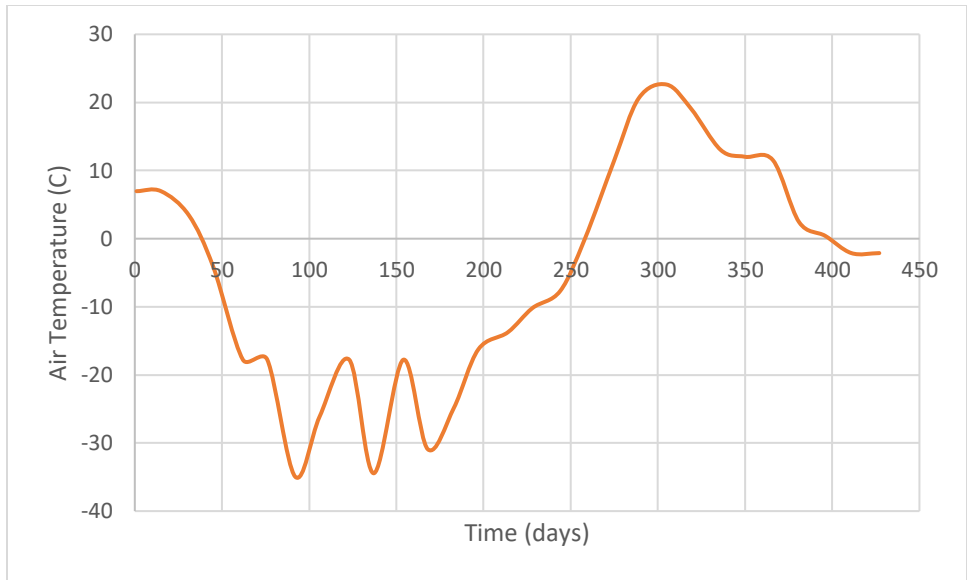


Figure 10.2: Air temperature vs. time

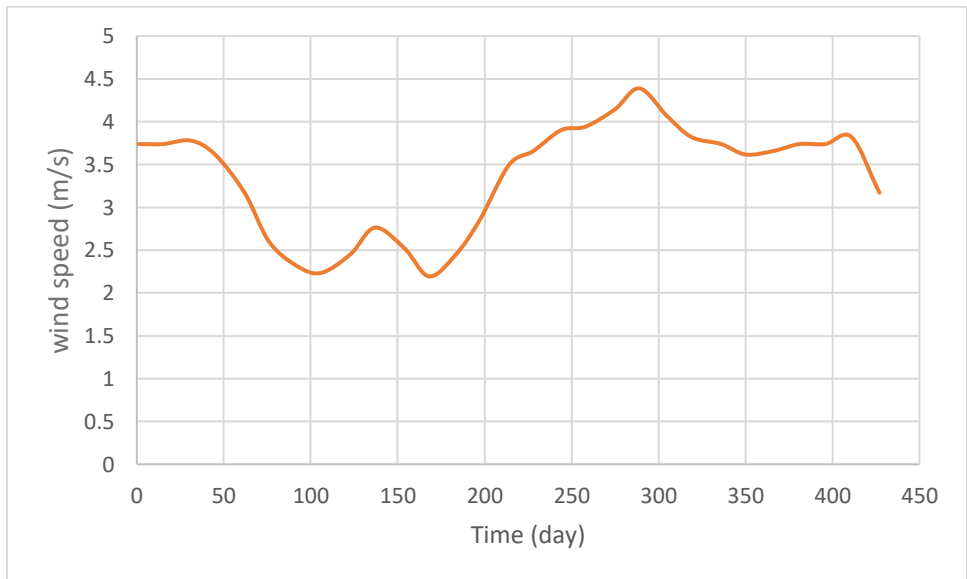


Figure 10.3: Wind speed vs. time

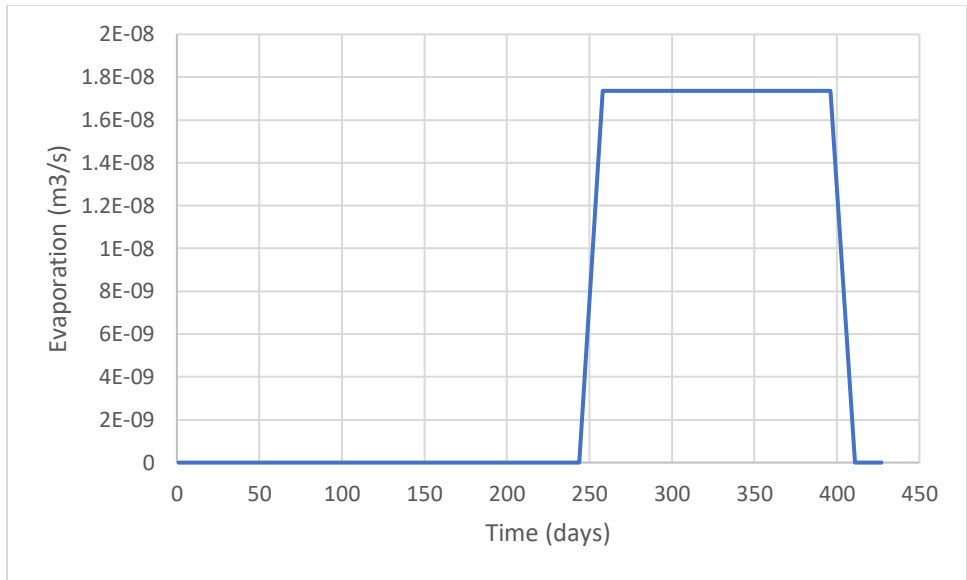


Figure 10.4: Evaporation vs. time

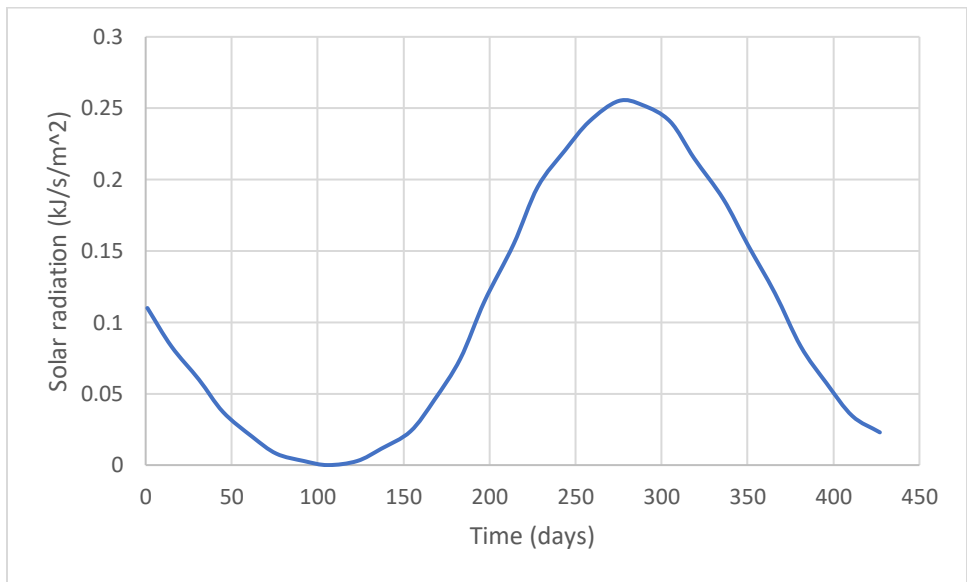


Figure 10.5: Solar radiation vs. time

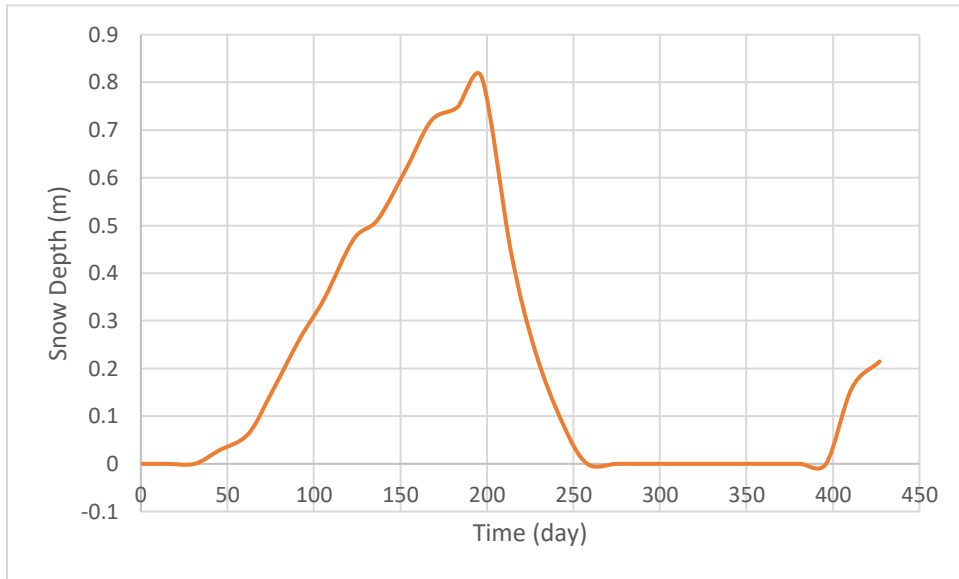


Figure 10.6: Snow depth vs. time

Table 10.3: Albedo vs. time

Time (days)	Albedo
<b>0</b>	0.15
<b>45</b>	0.5
<b>258</b>	0.15
<b>400</b>	0.15

Table 10.4: Vegetation height vs. time

Time (sec)	Vegetation Height (m)
<b>0</b>	0.001
<b>1e+09</b>	0.001

### 10.3. Material Properties

The column's soil stratigraphy consists of 7 soil types defined from ground surface as Peat, Silt 1, Silt 2, Silt 3, Silt 4, Grey silt and Grey Till. The material properties of the soils can be found in Table 10.5 and thermal Properties in Table 10.6.

Table 10.5: Material properties

Material name	Thickness (m)	Unit weight (kN/m <sup>3</sup> )	porosity	Hydraulic material behavior	Static water mode
Peat	0.122	1	0.99999	Drained	Dry
Silt 1	0.366	27	0.5	Drained	Dry
Silt 2	1.372	27	0.5	Drained	Dry
Silt 3	0.642	27	0.5	Drained	Dry
Silt 4	2.012	27	0.5	Drained	Dry
Grey silt	2.286	27	0.5	Drained	Dry
Grey till	23.840	27	0.5	Drained	Dry

Table 10.6: Thermal properties

Material name	Peat	Silt 1	Silt 2	Silt 3	Silt 4	Grey silt	Grey till
Static Temperature Mode	Grid	Grid	Grid	Grid	Grid	Grid	Grid
Water content	0.35	0.35	0.35	0.35	0.35	0.35	0.35
Thermal conductivity method	constant	constant	constant	constant	constant	constant	constant
Unfrozen Conductivity (kW/m/°C)	0.0004843	0.001038	0.0008302	0.001055	0.001176	0.001314	0.001851
Frozen conductivity (kW/m/°C)	0.001712	0.00192	0.001799	0.00192	0.001989	0.002041	0.002162
Latent Heat	yes	yes	yes	yes	yes	yes	yes
Unfrozen Volumetric Heat capacity (kJ/m3/°C)	3865	2224	2594	2224	2065	1959	1483
Frozen Volumetric Heat capacity (kJ/m3/°C)	2541	1483	1588	1483	1430	1430	1271

<b>Thermal soil unfrozen water content method</b>	Simple						
---	--------	--------	--------	--------	--------	--------	--------

## 10.4. Results

Figure 10.7 shows the temperature profile of the RS2 results compared with the Hwang (1976) prediction and measured data from field. RS2 shows good agreement with the prediction of Hwang (1976). The large temperature fluctuations near the ground surface are not predicted by RS2 and Hwang (1976) due to output being computed in time steps. It should also be noted that the location of the measured data has changed somewhat due to ground surface settlement.

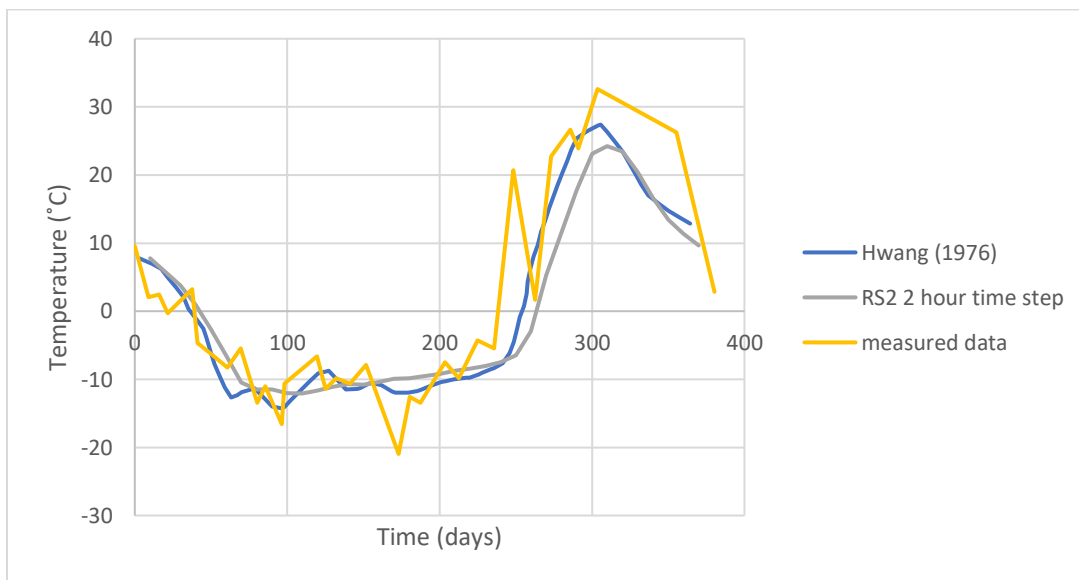


Figure 10.7: Comparison of RS2 results with Hwang (1976) and measured data

## 10.5. Reference

Hwang, C. (1976). Predictions and observations on the behaviour of a warm gas pipeline on permafrost. *Canadian Geotechnical Journal*, 13(4), pp.452-480.

# 11. Thermal Conductivity – Cote and Konrad

## 11.1. Introduction

This problem attempts to validate the RS2 implementation of thermal conductivity estimation using the Cote and Konrad (2005) approach. This approach integrates the effects of porosity, degree of saturation, mineral content, grain-size distribution, and particle shape on thermal conductivity of unfrozen and frozen soils. RS2 estimation of thermal conductivity will be compared to closed-form solution estimations by Cote and Konrad (2005), and experimental data collected by Kersten (1949).

## 11.2. Model Geometry

The RS2 model was designed to simulate the conditions of the experiment conducted by Kersten (1949). The unfrozen model comprises of a 1m column with an initial temperature of 20 °C. The frozen model comprises of a 1m column with an initial temperature -5 °C. For both the unfrozen and frozen model, pore pressure boundary condition for the top and bottom boundaries were set to 0 kPa and -100 kPa respectively.

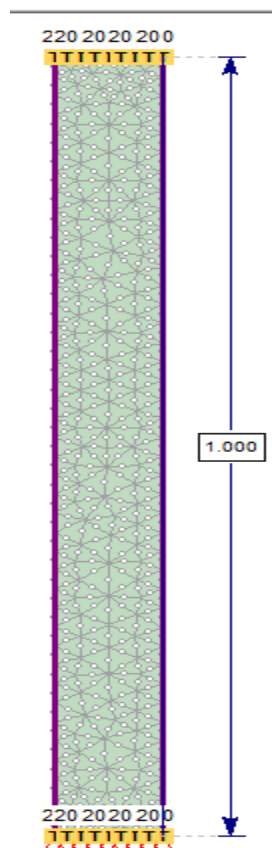


Figure 11.1: RS2 unfrozen model geometry

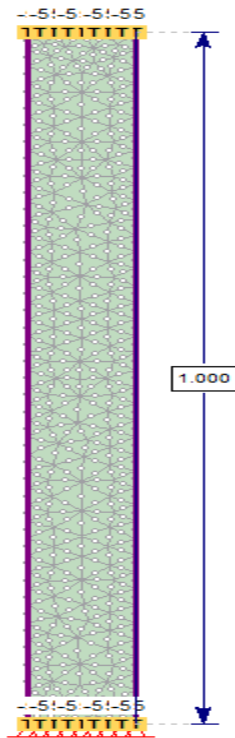


Figure 11.2: RS2 frozen model geometry

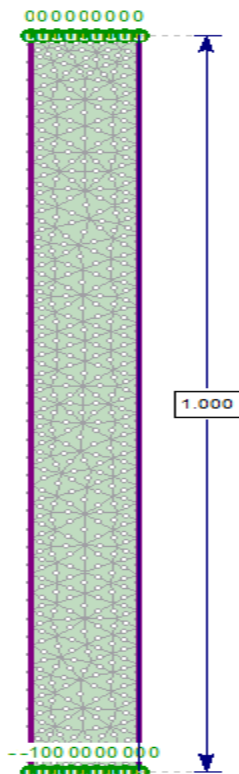


Figure 11.3: RS2 pore pressure boundary condition

## 11.3. Material Properties

The experiment set up by Kersten (1949) measured the thermal conductivity for two types of soils, Fairbanks sand sample and Healy clay sample. The soil properties used to model the experiment can be seen in Table 11.1 and Table 11.2.

Table 11.1: Material properties

Material name	Unit weight (kN/m <sup>3</sup> )	Porosity	Thermal conductivity method	Particle conductivity (W/m/C)	Unfrozen kappa	Frozen kappa	Chi (W/m/C)	Eta
<b>Fairbanks sand</b>	19.17	0.29	Cote and Konrad	5.3	4.6	1.7	0.75	1.2
<b>Healy clay</b>	15.66	0.42	Cote and Konrad	2.8	1.9	0.85	0.75	1.2

Table 11.2: User defined water content

Matric suction (kPa)	Water content (m <sup>3</sup> /m <sup>3</sup> )	
	Fairbank Sand	Healy Clay
<b>0</b>	0.29	0.42
<b>100</b>	1e-6	1e-06

It should be noted the volume fraction of unfrozen water that corresponds to the experimental data for frozen Healy clay sample is approximately 0.15. This is relevant for the accuracy of the frozen analysis solution. The additional parameters for Healy clay frozen model are included to reflect this data:

Table 11.3: Thermal soil unfrozen water content custom coordinates

Degrees (°C)	Unfrozen water content (m <sup>3</sup> /m <sup>3</sup> )
<b>-3</b>	0.15
<b>0</b>	0.42

## 11.4. Results

Figure 11.4 and Figure 11.5 **Error! Reference source not found.** show the RS2 estimation of thermal conductivity, along with Cote and Konrad (2005) closed-form solution estimation, and Kersten (1949) experiment data for unfrozen and frozen soil conditions respectively. Both figures show RS2 in good agreement with the closed-form solution and experiment data.

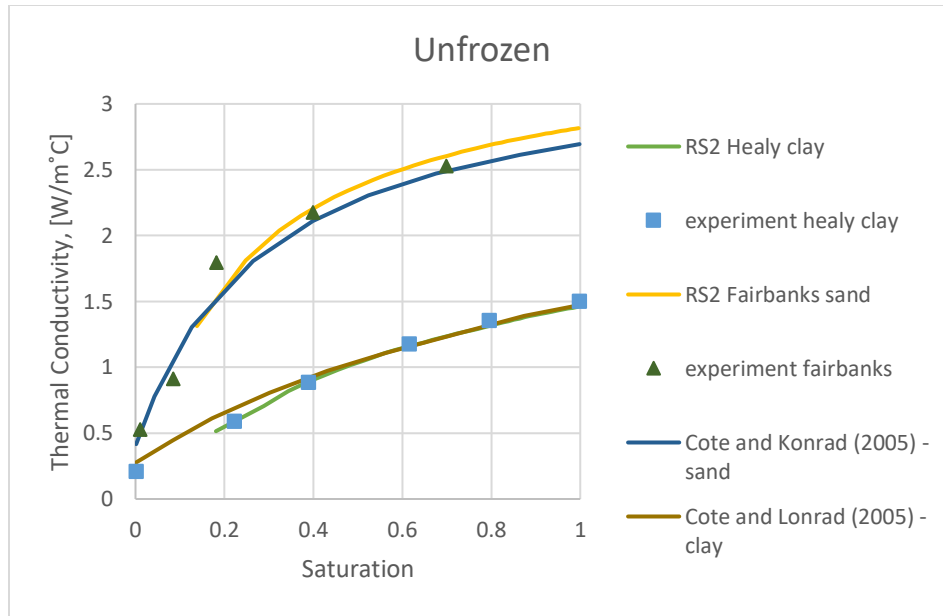


Figure 11.4: Unfrozen model comparison to estimated solution and experiment data

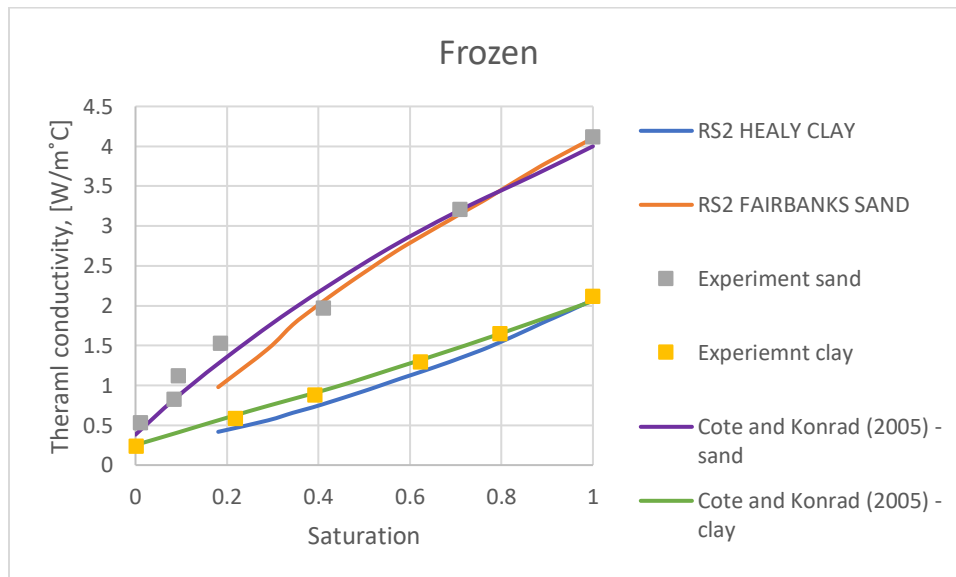


Figure 11.5: Frozen model comparison to estimated solution and experiment data

## 11.5. Reference

Côté, J. and Konrad, J. (2005). A generalized thermal conductivity model for soils and construction materials. *Canadian Geotechnical Journal*, 42(2), pp.443-458

Kersten, M.S. (1949). Laboratory research for the determination of the thermal properties of soils. *Research Laboratory Investigations, Engineering Experiment Station, University of Minnesota, Minneapolis, Minn. Technical Report 23.*

# 12. Thermal Conductivity Model – Johansen - Lu

## 12.1. Problem Description

This problem attempts to validate the RS2 implementation of thermal conductivity estimation using the Johansen (1975) model and the Lu et al. (2007) model. The behaviour of thermal conductivity with changing water content will be compared to experimental data collected. The RS2 model was designed to simulate the conditions of the experiment conducted by Lu et al. (2007) and Tarnawski et al. (2009). The model comprises of a 1m column with a constant initial temperature of 20°C. The top and bottom pore pressure boundary condition were set to 0 kPa and -100 kPa, respectively.

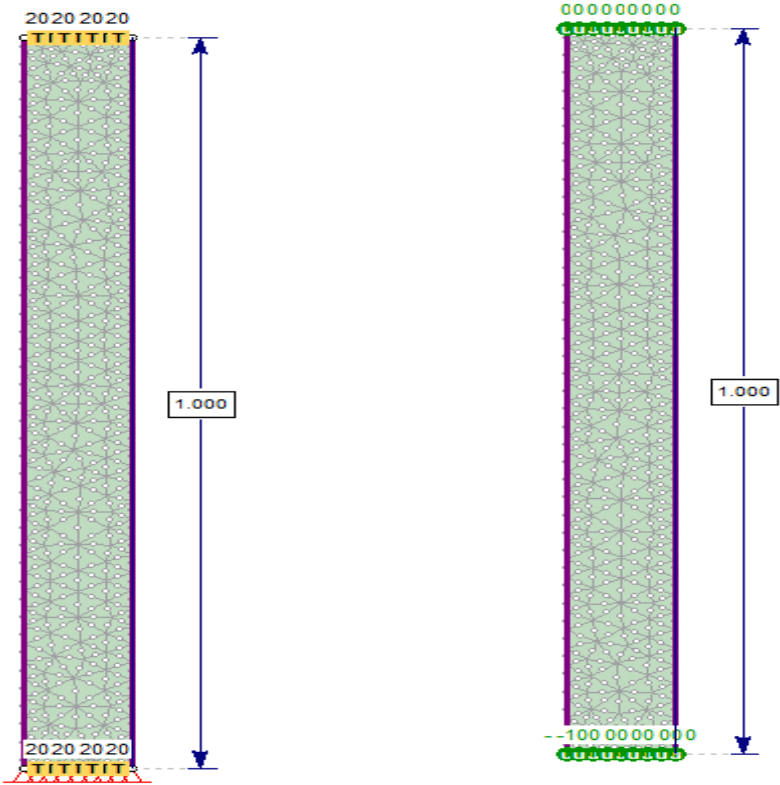


Figure 12.1: RS2 model geometry

## 12.2. Material Properties

The experiment set up by Lu et al. (2007) and Tarnawski et al. (2009) included four soil types with varying densities and quartz content. The soil properties used to model the experiment can be seen in Table 12.1.

Table 12.1: Material properties

Material name	Unit weight (kN/m <sup>3</sup> )	Porosity	Material type	Quartz content	Dry density (kg/m <sup>3</sup> )
Sand 1	15.696	0.407	coarse	0.74	1,600
Sand 2	15.696	0.407	coarse	0.51	1,600
Silty loam	13.047	0.5074	fine	0.47	1,330
Silty clay loam	12.753	0.518519	fine	0.36	1,300

Table 12.2: User defined water content

Matric suction	Water content
0	Porosity values of each material types
100	1e-06

### 12.3. Results

Figure 12.2 shows the results of the thermal conductivity calculated for each soil type by the Johansen and Lu model compared with the experimental data. The calculated results of both the Johansen and Lu are in good agreement with the experimental data.

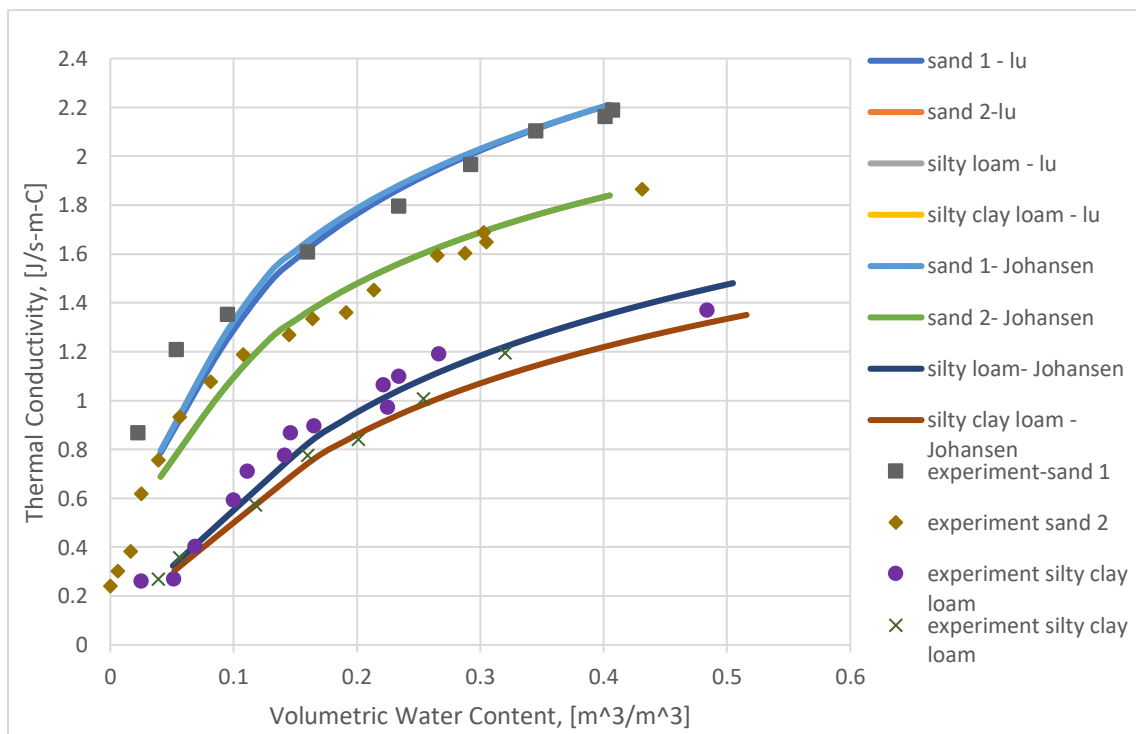


Figure 12.2: Comparison of thermal conductivity with varying Volumetric water content

## 12.4. References

Johansen, O. (1975). Thermal conductivity of soils. Ph.D. Thesis. *CRREL Draft Translation 637, 1977.*

Lu, S., Ren, T., Gong, Y., and Horton, R. (2007). An improved model for predicting soil thermal conductivity from water content at room temperature. *SSSAJ, 71 (1):8-14.*

Tarnawski, V.R., Momose, T., and Leong, W.H. (2009). Assessing the impact of quartz content on the prediction of soil thermal conductivity. *Geotechnique, 59(4): 331-338.*

# 13. Thermosyphon – Laboratory Test

## 13.1. Problem Description

Two asymmetric analysis was completed to simulate one of the laboratory experiments conducted by Haynes and Zarling (1988). Model 1 uses the manual thermosyphon method and model 2 uses the Haynes and Zarling method. This case demonstrates the thermosyphon modelling methods manual and Haynes and Zarling in RS2. The results will also be compared to that of TEMP/W.

## 13.2. Model Geometry

Each model has the same geometry. The domain comprises of a height 6.1m and width 0.325m. The left boundary represents the outside surface of the evaporator and is 0.025m (outside radius of evaporator) from the central axis  $x=0$ . The left boundary is assigned a vertical infiltration of 20 m/s and the thermosyphon boundary condition. The right boundary represents the inside surface of the outer pipe that contains the fluid and evaporator. The right boundary is assigned a constant pore pressure and temperature of 20kPa and 20°C, respectively. The analysis is taken over the period of 10800 s with staging in increments of 3600 s.

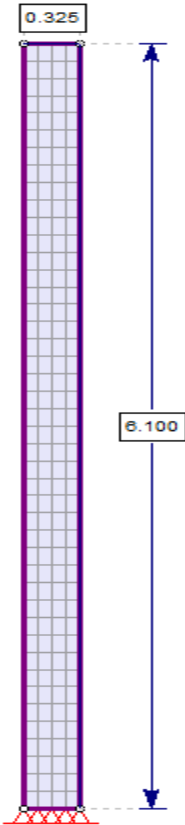


Figure 13.1: RS2 model geometry

### 13.3. Material Properties

The material properties of the column can be seen in Table 13.1. Table 13.2 shows thermosyphon properties used. Figure 13.2 shows the convection coefficient function used in model 1 and Figure 13.3 shows the wind speed function.

Table 13.1: Material properties

Parameter	Value
<b>Porosity</b>	0.999999
<b>Thermal conductivity</b>	Simple
<b>Frozen conductivity (kW/m/C)</b>	0.0005
<b>Unfrozen conductivity (kW/m/C)</b>	0.0005
<b>Thermal volumetric heat capacity</b>	constant
<b>Latent heat</b>	No
<b>Unfrozen heat capacity (kJ/m<sup>3</sup>/C)</b>	4
<b>Frozen heat capacity (kJ/m<sup>3</sup>/C)</b>	4
<b>Thermal soil unfrozen water content</b>	simple
<b>Thermal expansion</b>	No
<b>Dispersivity</b>	No

Table 13.2: Thermosyphon properties

Parameter	Value
<b>Air temperature method</b>	Constant
<b>Air temperature value (C)</b>	-18
<b>Delta temperature (C)</b>	1
<b>Max temperature (C)</b>	-0.5
<b>Model 1</b>	
<b>Method</b>	Manual
<b>Heat capacity method</b>	Wind dependant
<b>Perimeter (m)</b>	0.1
<b>Model 2</b>	
<b>Method</b>	Zarling and Haynes

<b>Gas type</b>	CO2
<b>Angle (degrees)</b>	12
<b>Wind speed method</b>	Time dependant
<b>Radiator area (m2)</b>	1
<b>Syphon length (m)</b>	1
<b>Perimeter (m)</b>	0.1

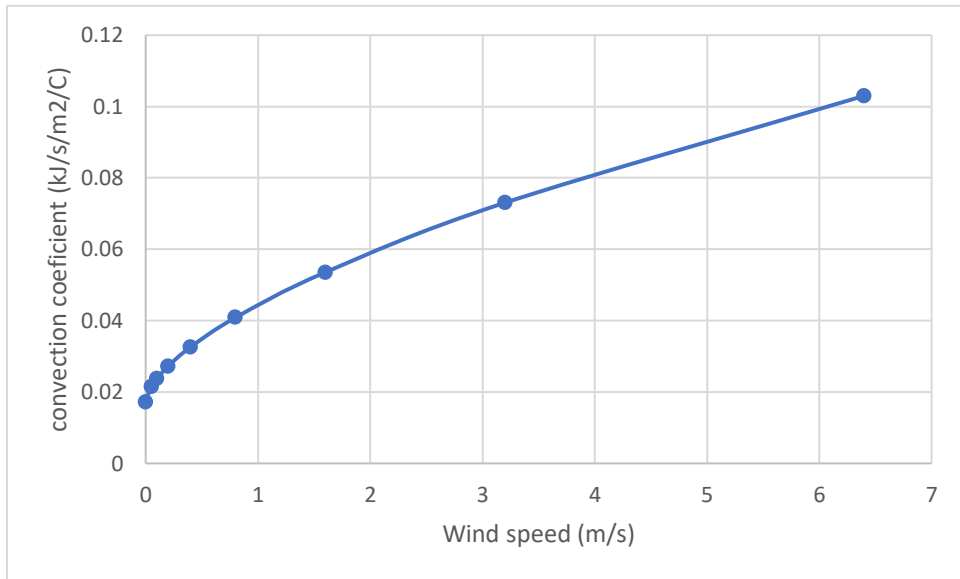


Figure 13.2: Convection coefficient function

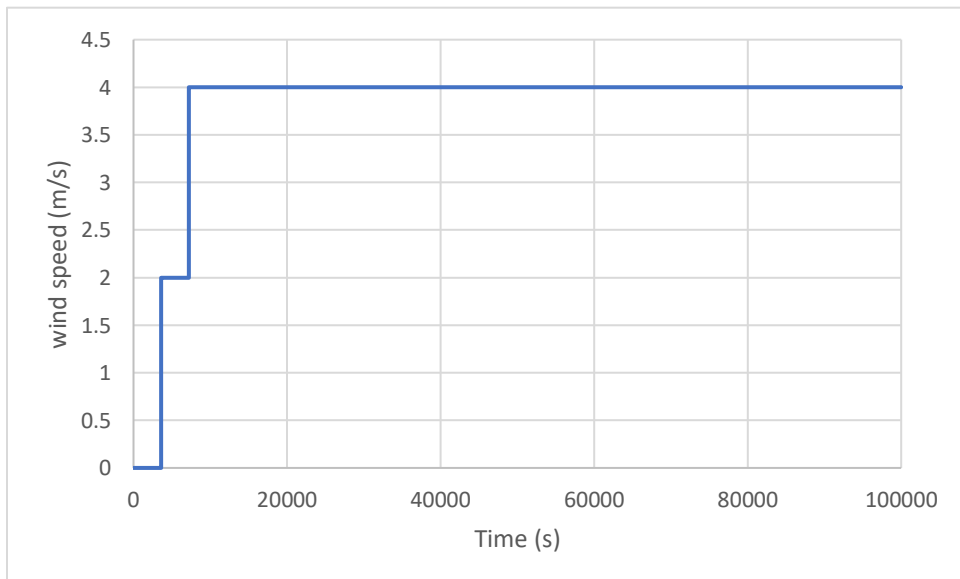


Figure 13.3: Wind speed function

## 13.4. Results

Figure 13.4 shows the temperature history at the surface of the evaporator for RS2 model 1,2 and TEMP/W. The results show good agreement between all models. Figure 13.5 presents the total heat rate of the thermosyphon. The value obtained after computation is multiplied by Pi value to obtain a full revolution about the axis of symmetry.

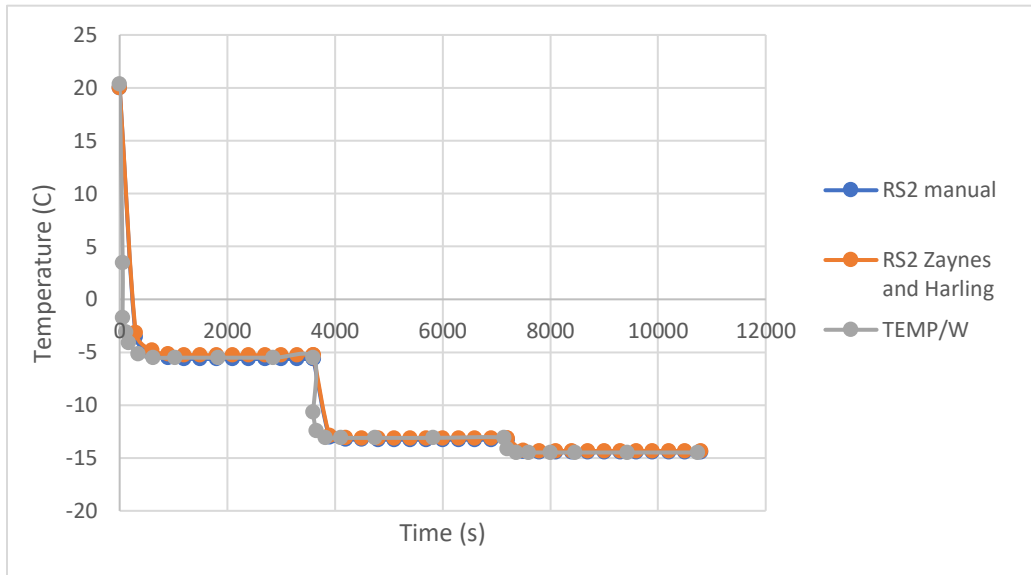


Figure 13.4: Temperature history at evaporator surface

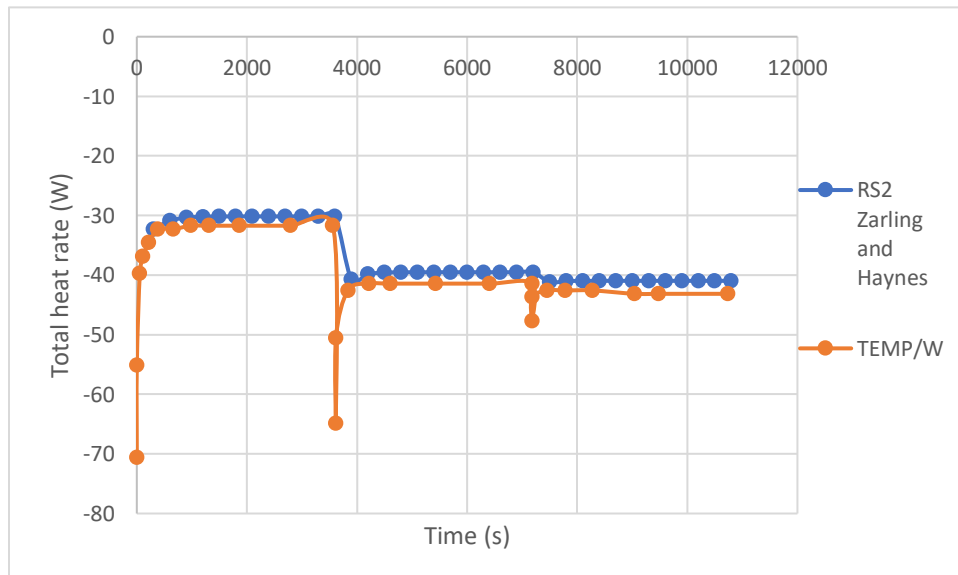


Figure 13.5: Total heat rate at the thermosyphon

## 13.5. References

Haynes, F.D. and Zarling, J.P. (1988). Thermosyphons and foundation design in cold regions. *Cold Regions Science and Technology*, 15, 251-259. Elsevier Science Publishers B.V. Amsterdam.

# 14. Thermosyphons in Pipeline Piles

## 14.1. Problem Description

This example demonstrates RS2 ability to model the effect of thermosyphons inside steel piles to prevent degradation of permafrost. This an asymmetric analysis. The results of this analysis will be compared to that of TEMP/W. The model domain is 6m wide and 8m in height. The steel pipe pile is approximately 0.4m in diameter and steel wall thickness of 25mm. Only half of the pile is modelled (Figure 14.1). The analysis will take place over a 4-year period with an initial temperature of -4°C. The first three years of climate cycles is necessary to obtain realistic initial thermal conditions.

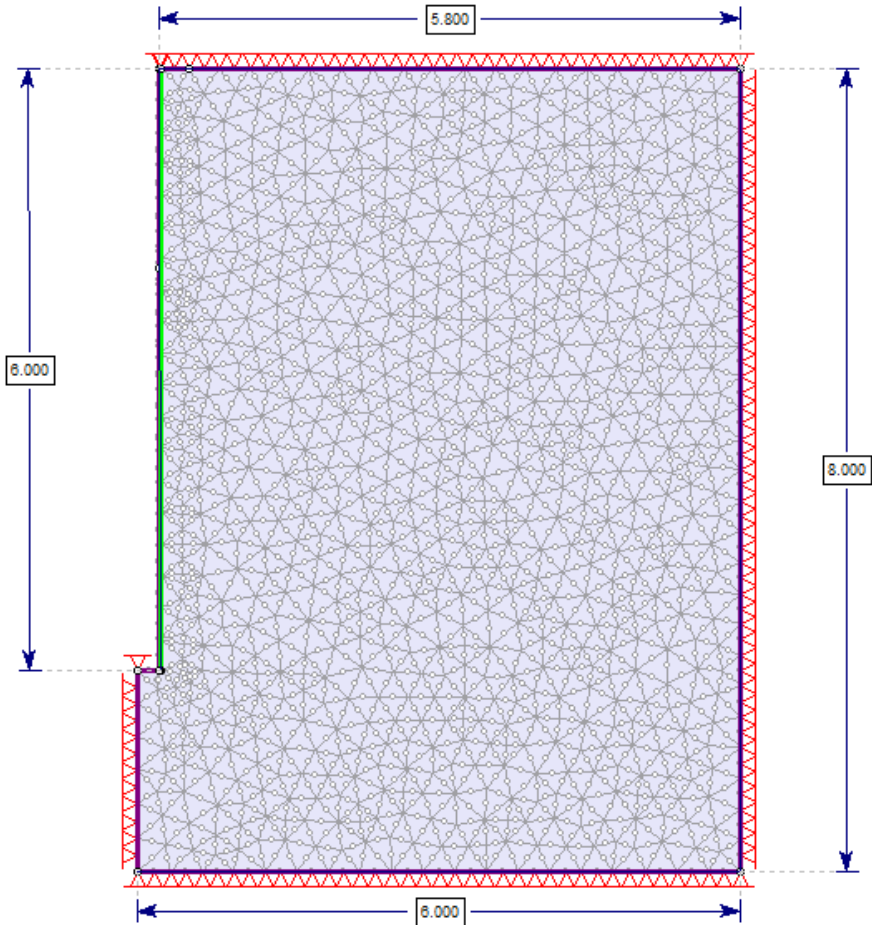


Figure 14.1: RS2 model geometry

The thermosyphon in the pile is 4m length from the bottom of the pile. The flux simulating climate condition will be set at the top boundary and to account for additional heat conduction into the ground through the steel pile, the air temperature function (Figure 14.5) is applied to the top of the pile. The temperature at the bottom boundary is kept at a constant temperature of -4 °C.

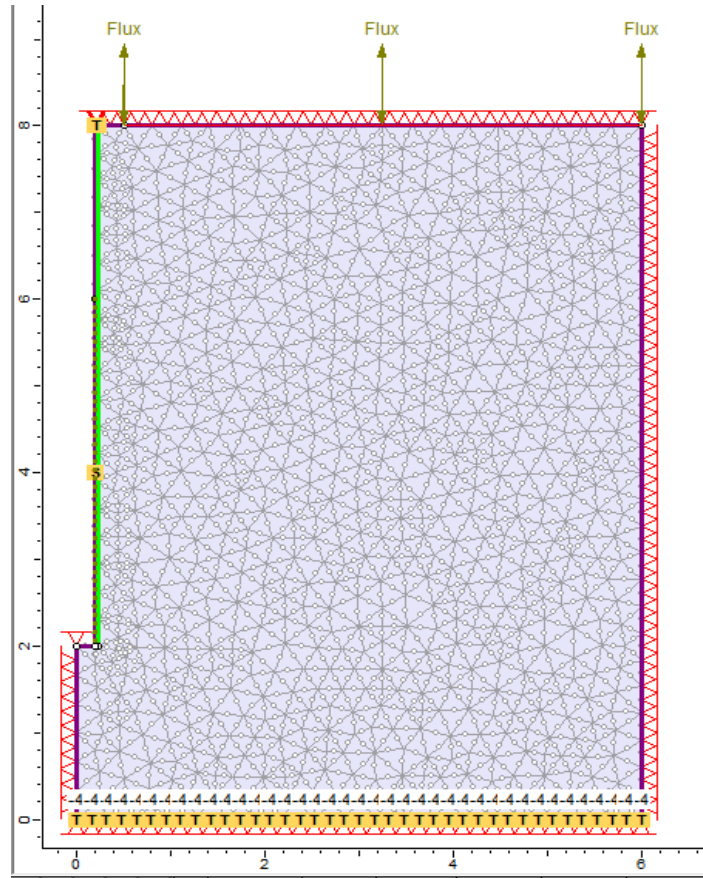


Figure 14.2: Transient model conditions

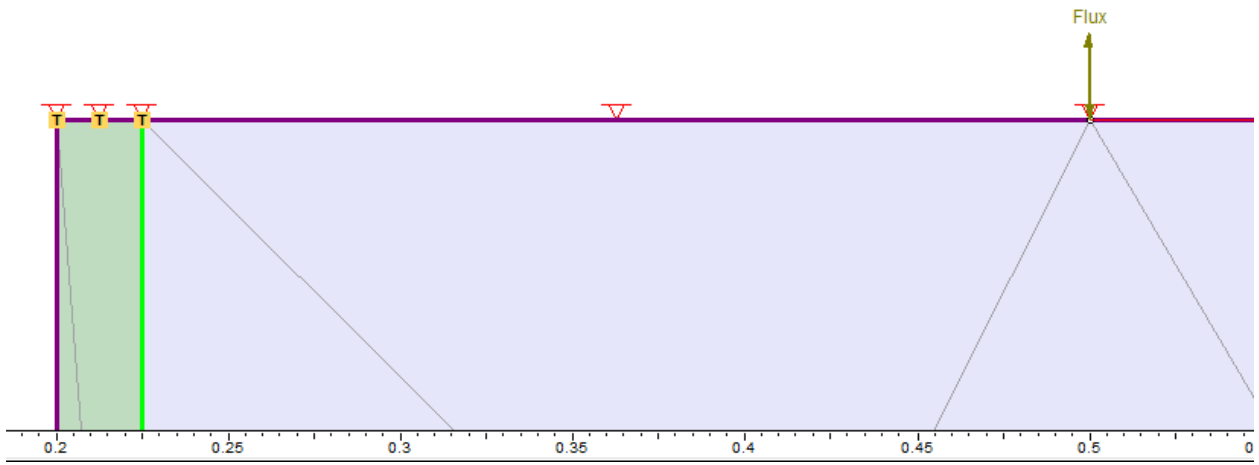


Figure 14.3: Top boundary conditions

## 14.2. Model Properties

The properties of the soil and pipe steel wall can be found in Table 14.1. The unfrozen water content function is seen in Figure 14.4.

Table 14.1: Material properties

Material	Parameters	Value
<b>Soil</b>	<b>Thermal Properties</b>	
	Water content	0.4
	Thermal Conductivity method	Constant
	Unfrozen Conductivity (kW/m/ °C)	0.00173611
	Frozen conductivity (kW/m/ °C)	0.00173611
	Frozen temperature	0
	Thermal volumetric heat capacity type	Constant
	Include latent heat	Yes
	Unfrozen heat capacity (kJ/m <sup>3</sup> / °C)	2400
	Frozen heat capacity	2400
	Thermal soil unfrozen water content type	Custom
<b>Steel</b>	<b>Thermal Properties</b>	
	Water content	0
	Thermal Conductivity method	Constant
	Unfrozen Conductivity (kW/m/ °C)	0.05
	Frozen conductivity (kW/m/ °C)	0.05
	Frozen temperature	0
	Thermal volumetric heat capacity type	Constant
	Include latent heat	No
	Unfrozen heat capacity (kJ/m <sup>3</sup> / °C)	3800
	Frozen heat capacity	3800
	Thermal soil unfrozen water content type	Simple

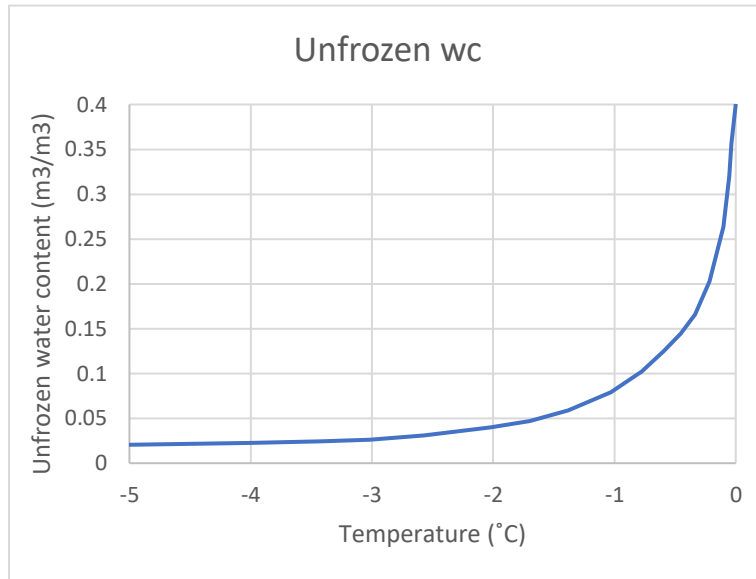


Figure 14.4: Unfrozen water content function

The climate annual climate data used is as follows.

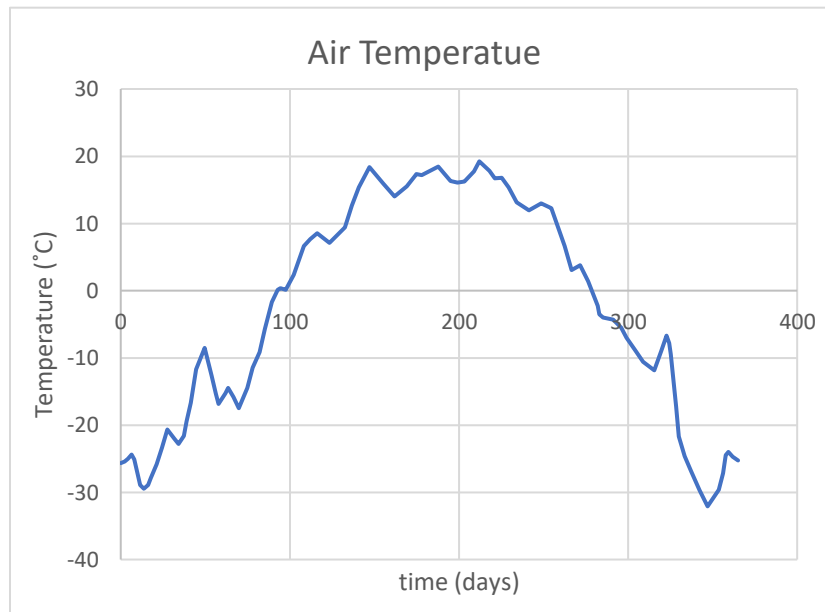


Figure 14.5: Mean daily air temperature

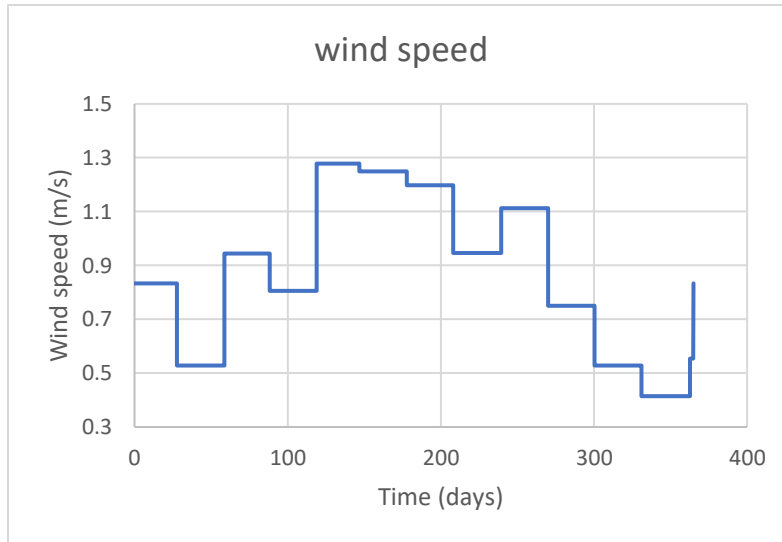


Figure 14.6: Average monthly wind speed

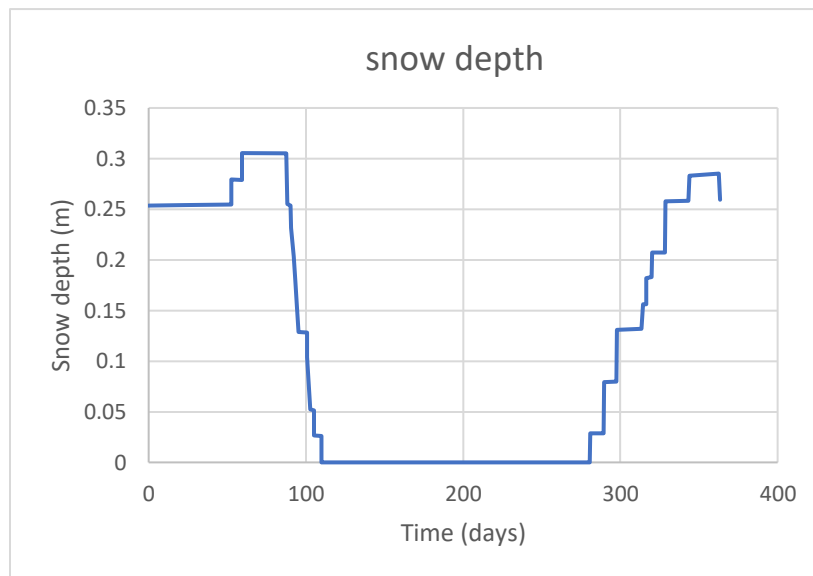


Figure 14.7: Average snow depth function

When there is no snow (day 110 to day 280) the albedo is set to 0.9. When there is snow on the surface the albedo is 0.3 as seen in Figure 14.8. The solar radiation function is estimated for latitude 65 °N.

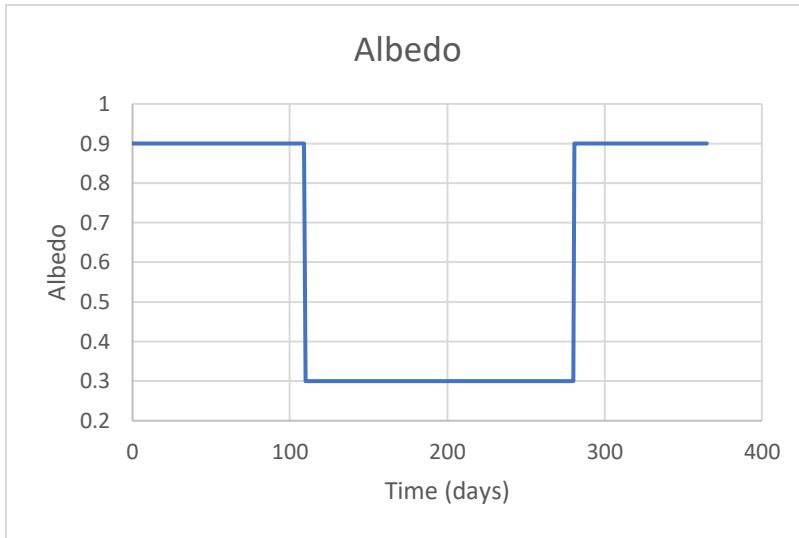


Figure 14.8: Albedo function

The snow conductivity is 0.000116 kJ/sec/m/ °C. Table 14.2 shows the thermosyphon properties and Figure 14.9 the heat transfer function.

Table 14.2: Thermosyphon properties

Type	Data
<b>Air temperature method</b>	Time dependent
<b>Method</b>	Manual
<b>Heat capacity method</b>	Time dependent

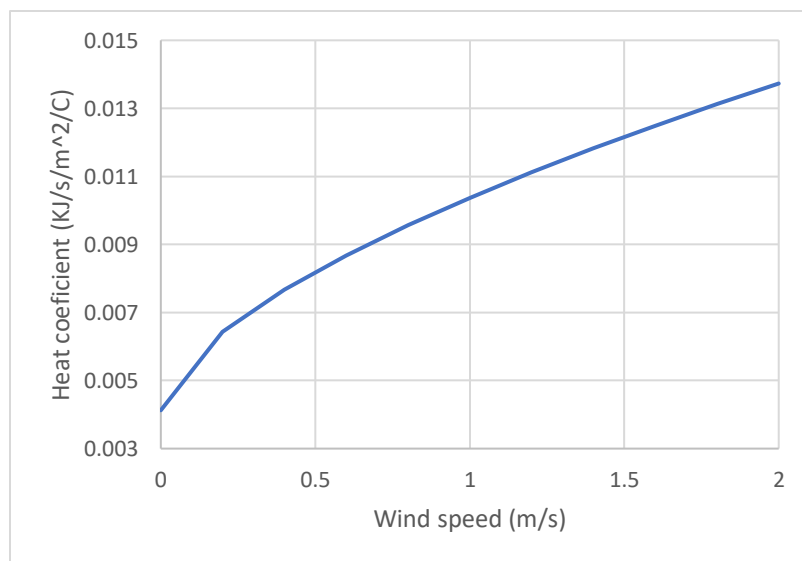


Figure 14.9: Thermosyphon heat transfer function

### 14.3. Results

Figure 14.10 through Figure 14.14 show the temperature contours of RS2 and TEMP/W in the range of -26 °C to 0 °C. Both TEMP/W and RS2 show the same trends but temperature contour differences are seen due to differing time steps in each program. The discussion follows the results seen by RS2.

In early February, most of the ground is frozen (Figure 14.10). The ground temperature is lower near the activated thermosyphon. By the 10<sup>th</sup> day of April, the ground is beginning to thaw, the temperatures only range from -4 °C to 0 °C (Figure 14.11). By the beginning of July, the majority of the upper two meters has thawed (Figure 14.12). It should be noted that the depth of unfrozen soil is greater furthest from the thermosyphon and pile. At the start of October, the temperatures begin to drop again, and the ground surface is beginning to freeze again (Figure 14.13). Note the soil immediately next to the pile freezes faster. By the end of December, all the soil next to the thermosyphon is frozen (Figure 14.14). Further away from the thermosyphon and pile is still a pocket of unfrozen soil.

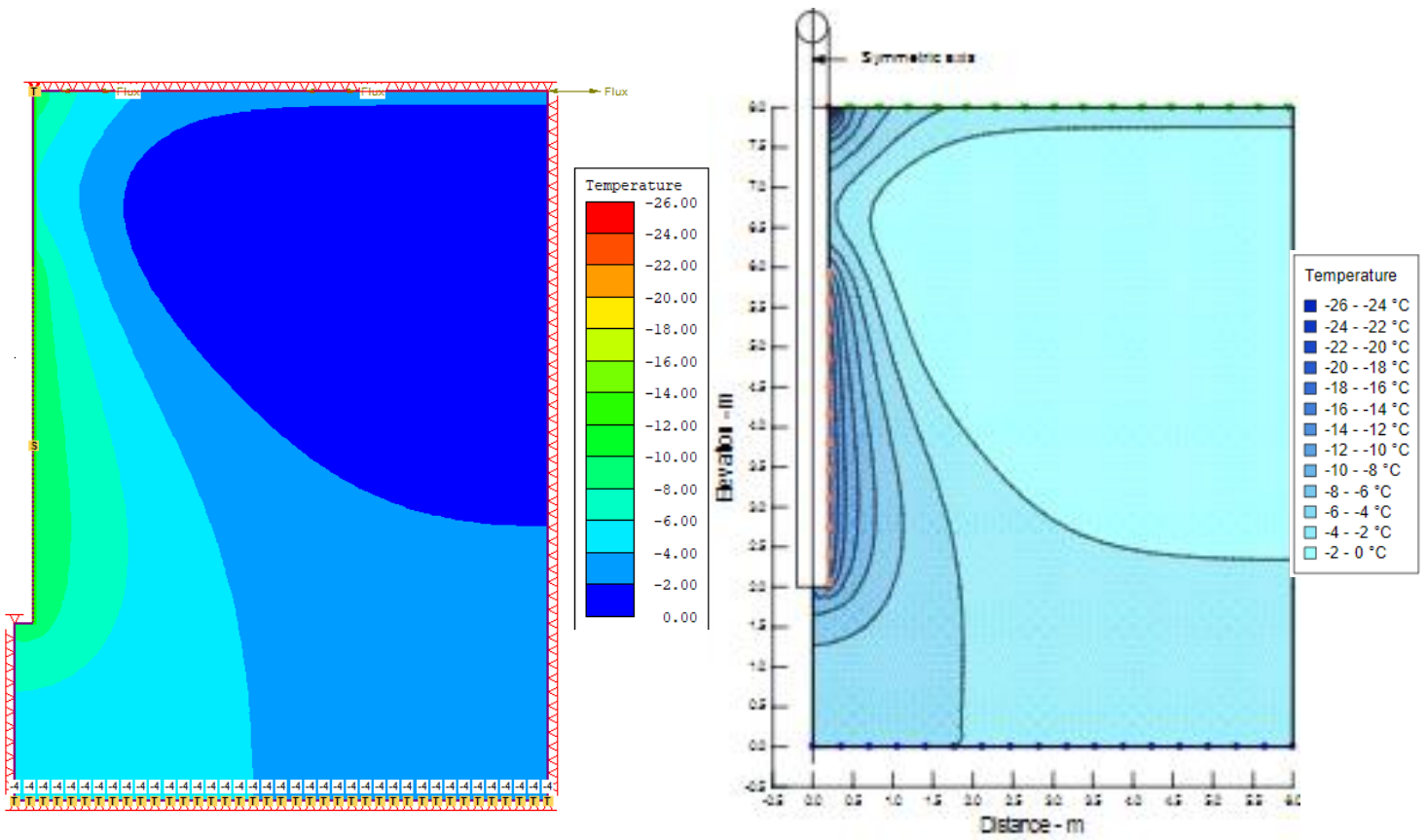


Figure 14.10: a) Temperature profile on the 15<sup>th</sup> day of February in RS2  
 b) Temperature profile early February in TEMP/W

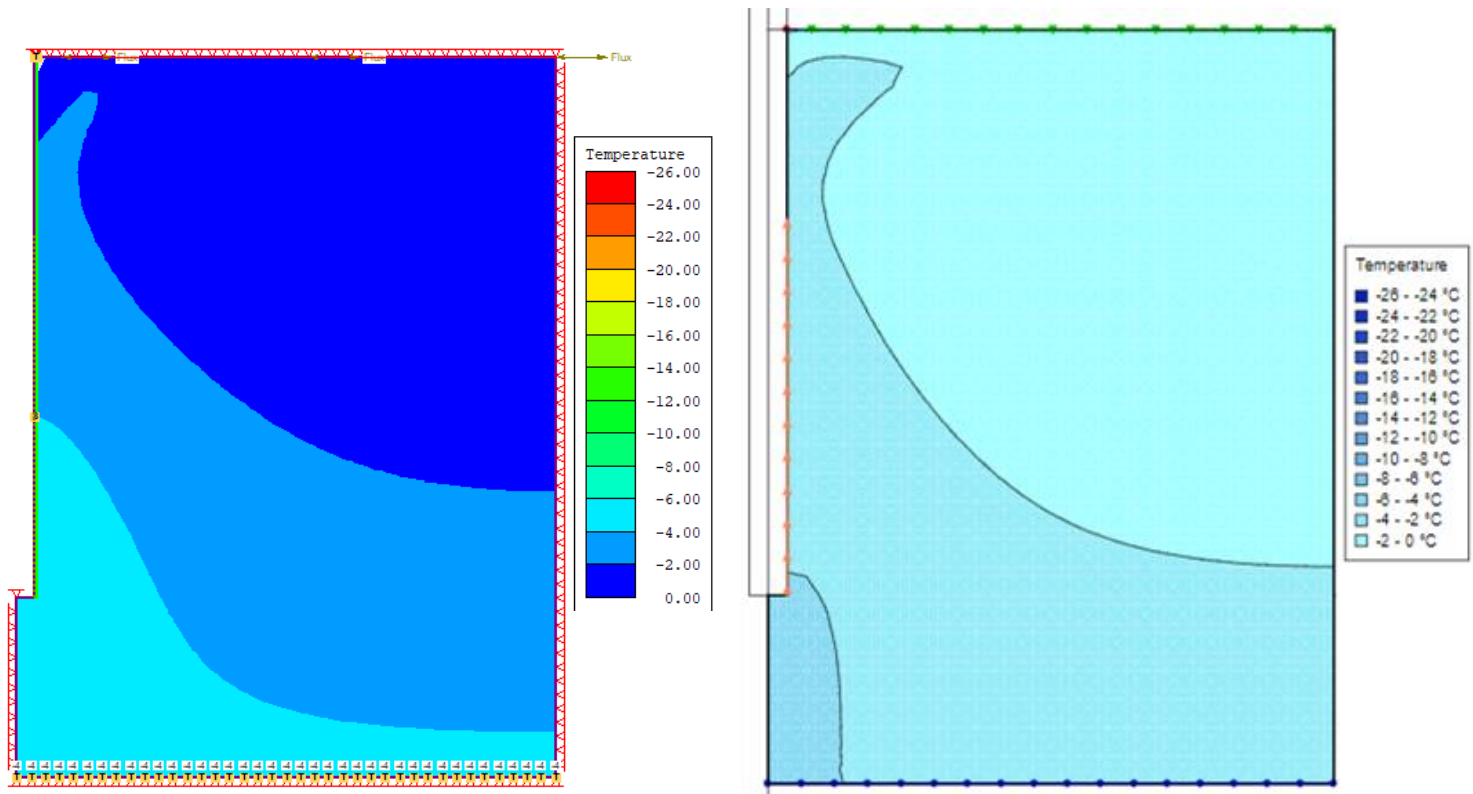


Figure 14.11: a) Temperature profile on the April 10<sup>th</sup> in RS2  
 b) Temperature profile early April in TEMP/W

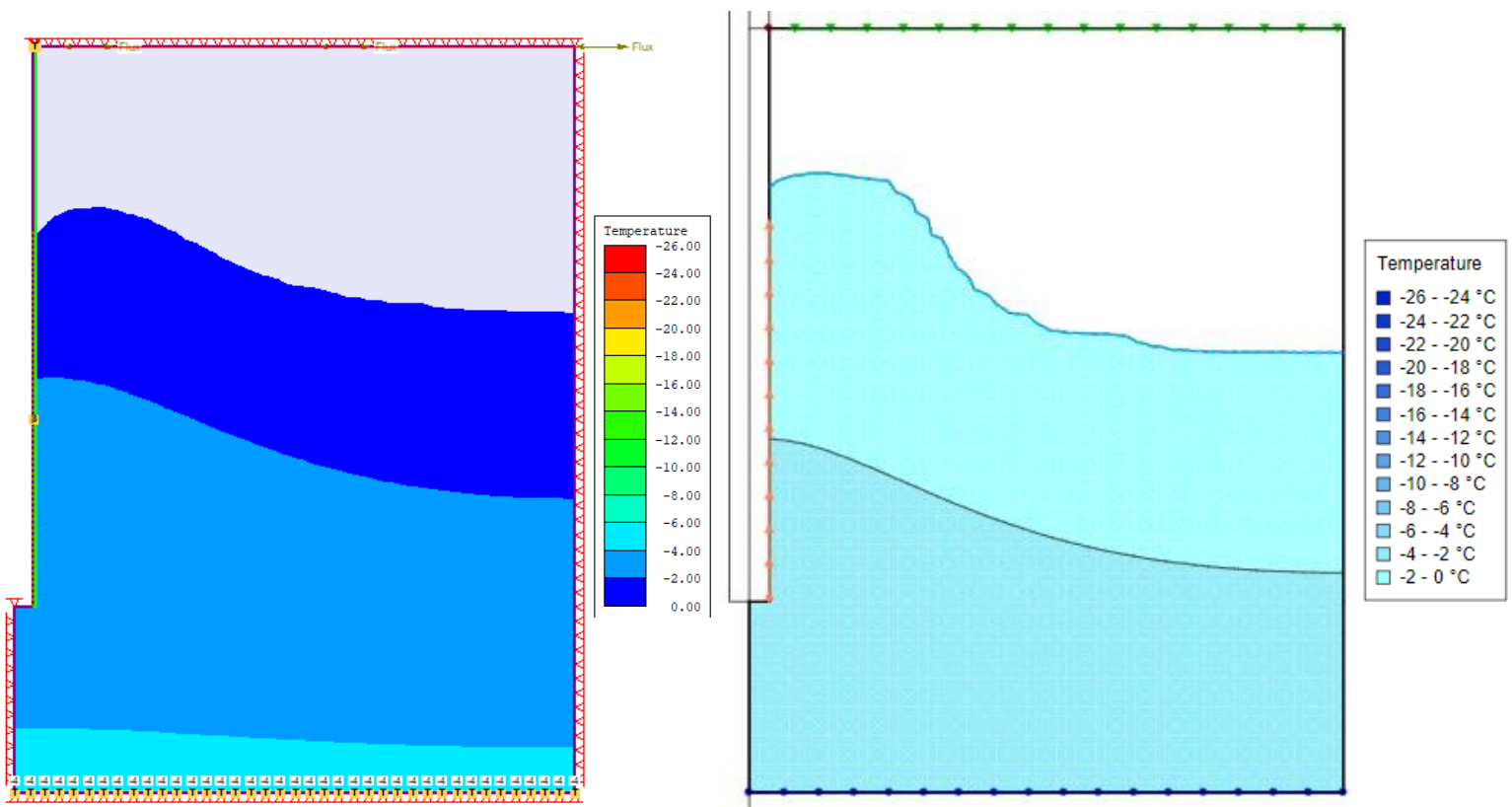


Figure 14.12: Temperature profile at the beginning of July: a) RS2 b) TEMP/W

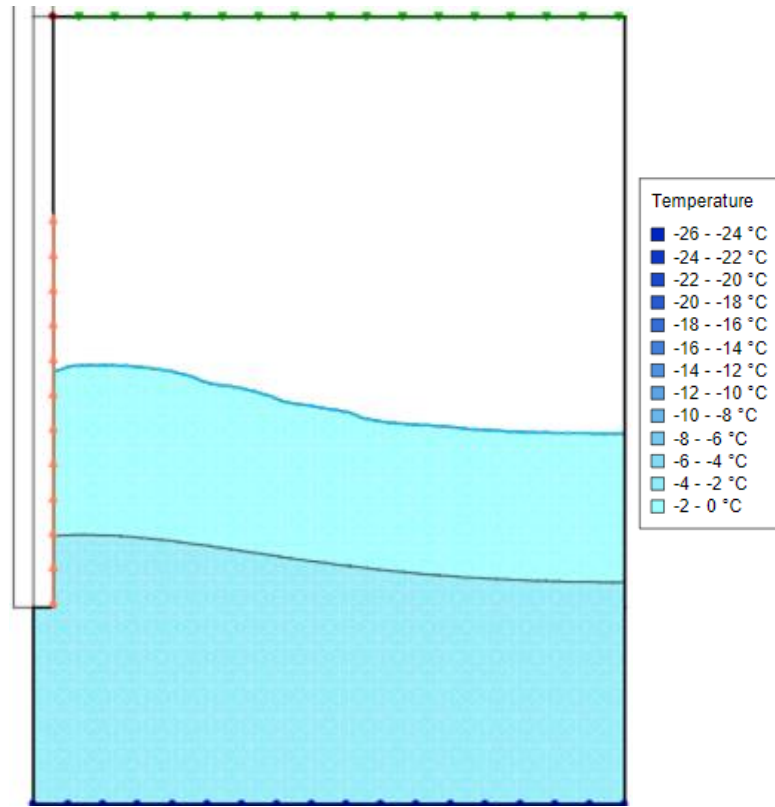
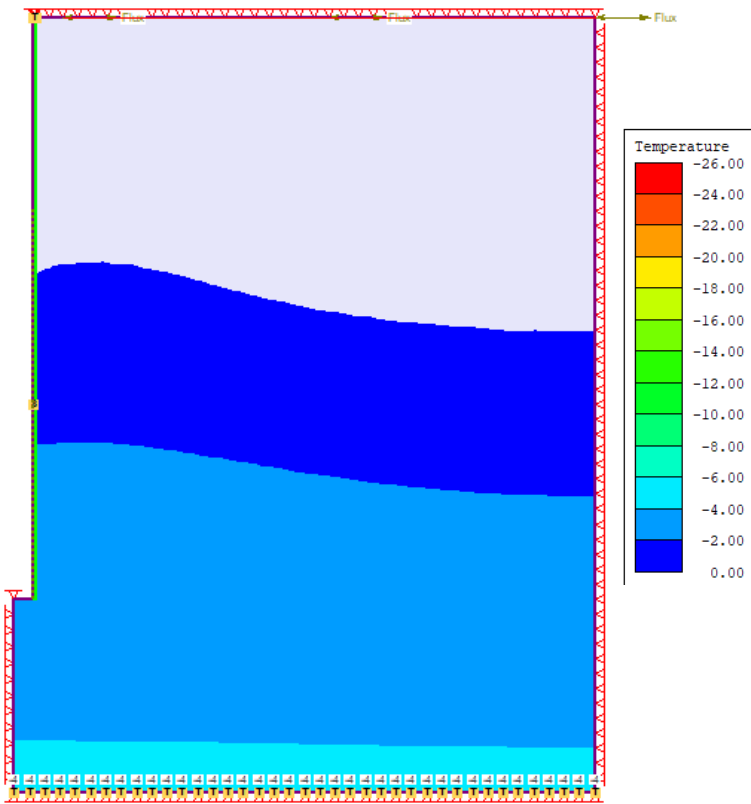


Figure 14.13: Temperature profile at the beginning of October: a) RS2 b) TEMP/W

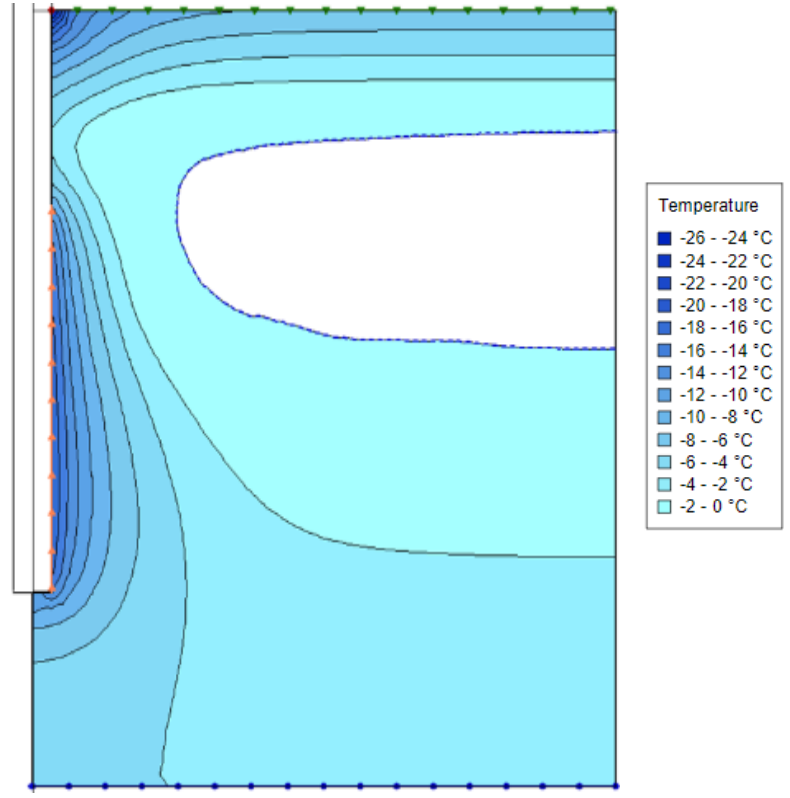
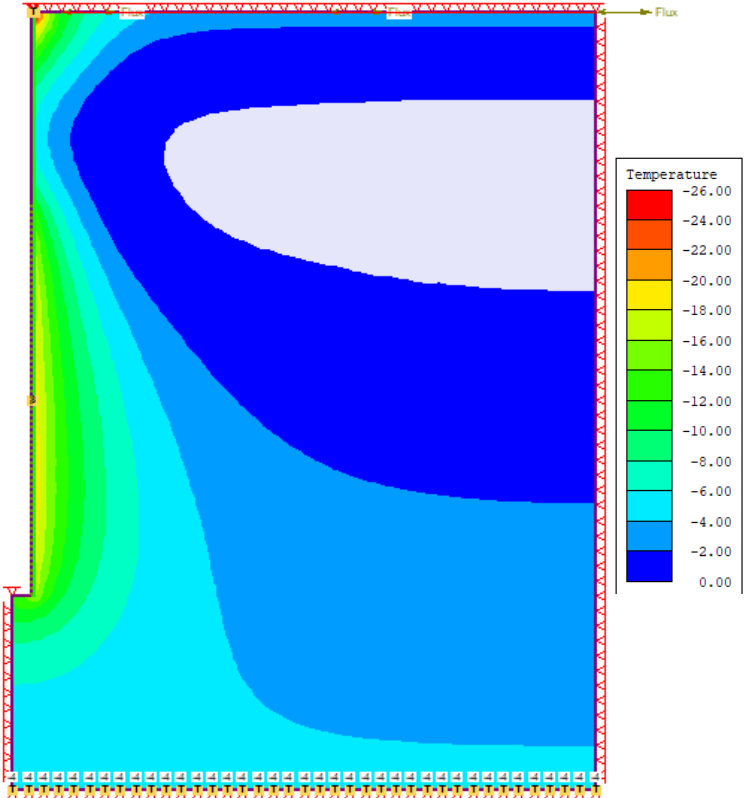


Figure 14.14: Temperature profile at the end of December: a) RS2 b) TEMP/W

## 14.4. References

GEO-SLOPE International Ltd. (n.d.). Temp/W example models. *Thermosyphon in pipe*.

# 15. Thermal Expansion – 2D

## 15.1. Problem Description

To verify capacity of RS2 for thermal expansion analysis, a simple model was created to verify the accuracy of thermal strain calculation of solid elements. Geometry and boundary conditions of the model are shown in Figure 15.1. Material properties are shown in Table 15.1. The whole model was set an initial temperature of 125 Celsius degrees at the initial stage. Then the temperature increases to 250 degrees and 500 degrees at second and third stage respectively.

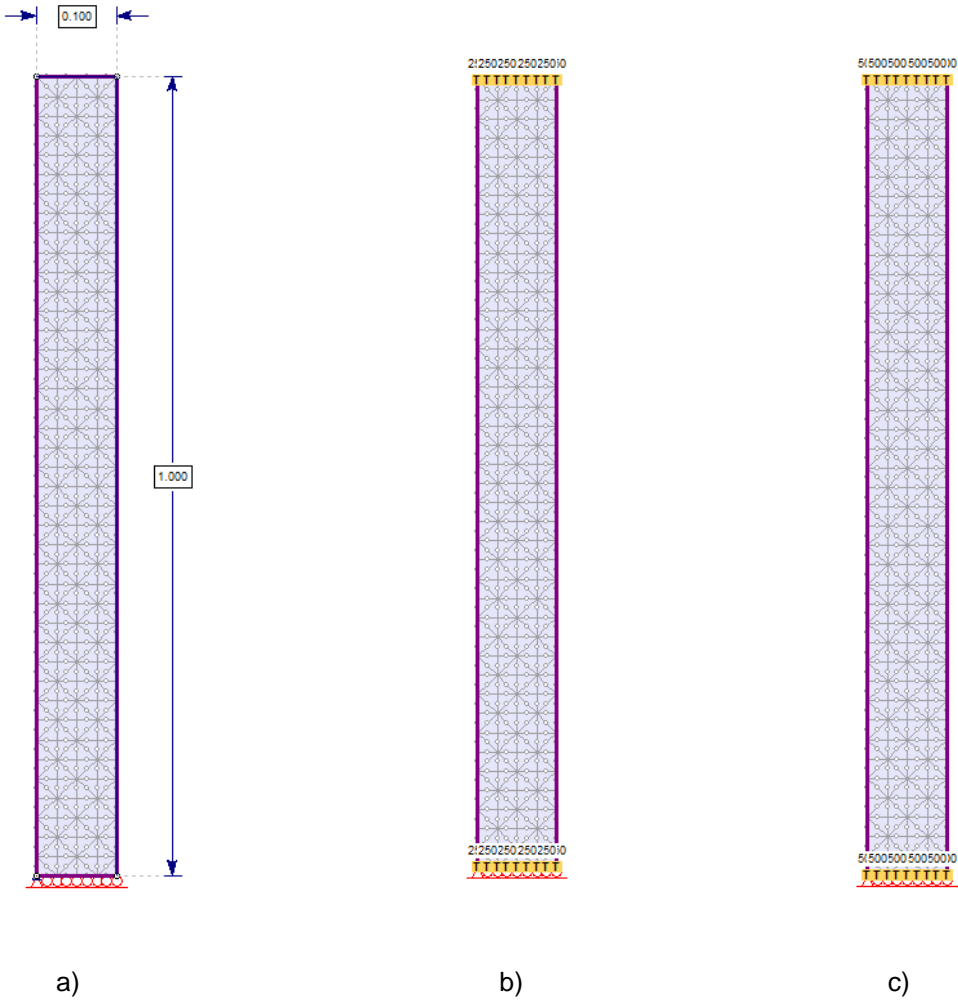


Figure 15.1: RS2 model. a) Geometry b) Stage 2 Thermal BC c) Stage 3 Thermal BC

Table 15.1: Model properties

Parameters	Value
<b>Initial Conditions</b>	
Unit weight (kN/m <sup>3</sup> )	20
Initial Temperature (Celsius)	125
<b>Thermal Properties</b>	
Thermal expansion Linear Coefficient (m/m/C)	1e-5
Unfrozen Conductivity	1
Frozen conductivity	1

## 15.2. Analytical Solution

The thermal strain is calculated as

$$\Delta\varepsilon^{ii} = \alpha\Delta T \quad (15.1)$$

where  $\Delta\varepsilon$  is the principal thermal strain vector,  $\alpha$  is the thermal expansion linear coefficient and  $\Delta T$  is the changes in temperature.

For stage 2, thermal strain is  $1e-5 \times 125 = 0.00125$  and stage 3 thermal strain is  $1e-5 \times 375 = 0.00375$

## 15.3. Results

Figure 15.2 shows the vertical displacement computed in RS2. The results indicate strong agreement with the analytical solution.

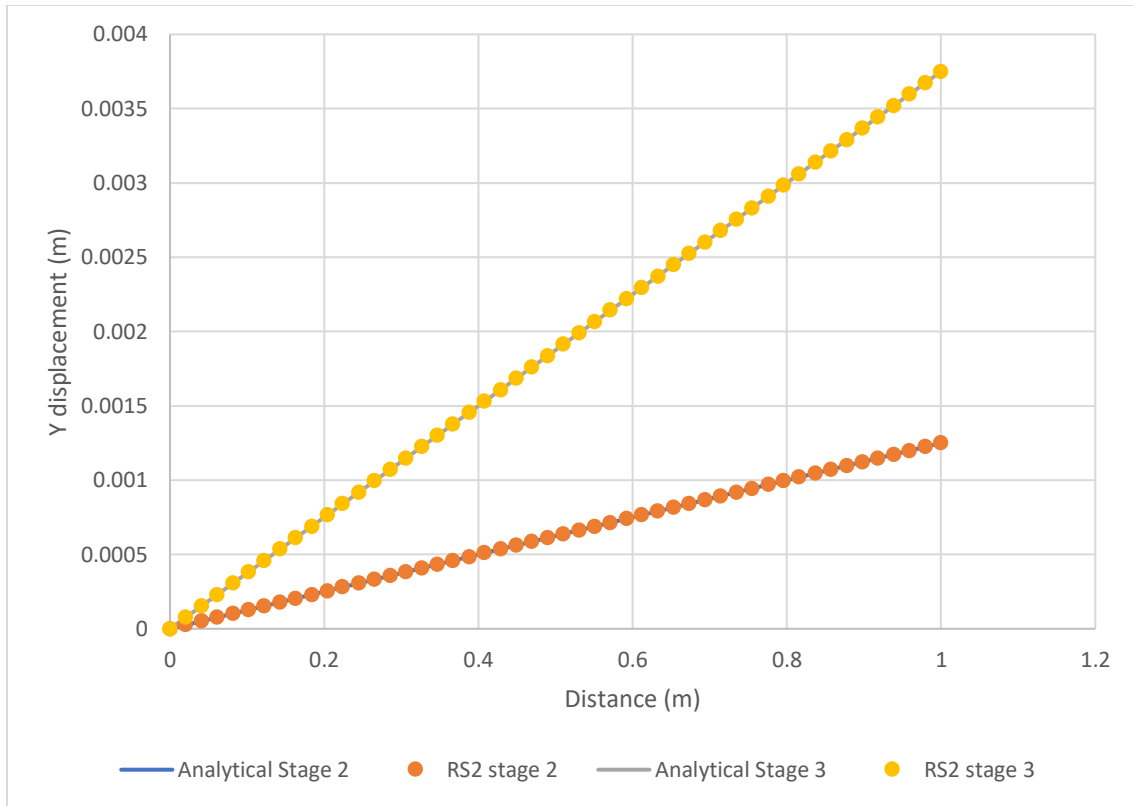


Figure 15.2: Vertical displacement in Y direction

# 16. Thermal Expansion – 1D

## 16.1. Problem Description

To verify capacity of RS2 for thermal expansion analysis, a simple model was created to verify the accuracy of thermal strain calculation of beam elements. Geometry and boundary conditions of the model are shown in Figure 16.1. Material properties are shown in Table 16.1. The whole model was set with an initial temperature of 20 Celsius degrees at the initial stage. Then the temperature increases to 60 degrees at the second stage.

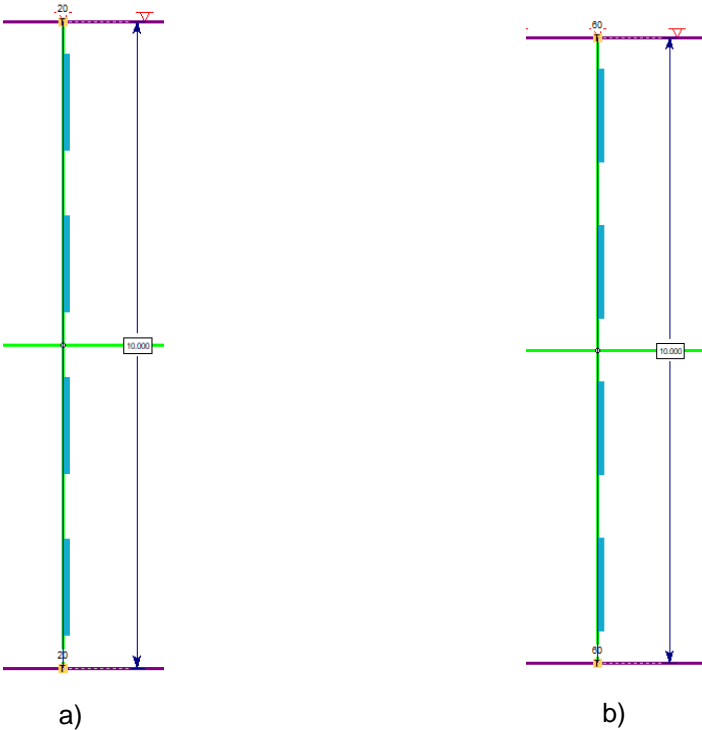


Figure 16.1: RS2 model. a) Geometry b) Stage 2 Thermal BC

Table 16.1: Model properties

Parameters	Value
<b>Initial Conditions</b>	
Unit weight (kN/m <sup>3</sup> )	77
Initial Temperature (Celsius)	20
<b>Thermal Properties</b>	
Thermal expansion Linear Coefficient (m/m/C)	5e-5
Conductivity (W/m/C)	30

## 16.2. Analytical Solution

The thermal strain is calculated as

$$\Delta\varepsilon^{ii} = \alpha\Delta T \tag{ 16.1 }$$

where  $\Delta\varepsilon$  is the principal thermal strain vector,  $\alpha$  is the thermal expansion linear coefficient and  $\Delta T$  is the changes in temperature.

For stage 2, thermal strain is  $5e-5 \times 40 = 0.002$

## 16.3. Results

Figure 16.2 shows the vertical displacement computed in RS2. The results indicate strong agreement with the analytical solution.

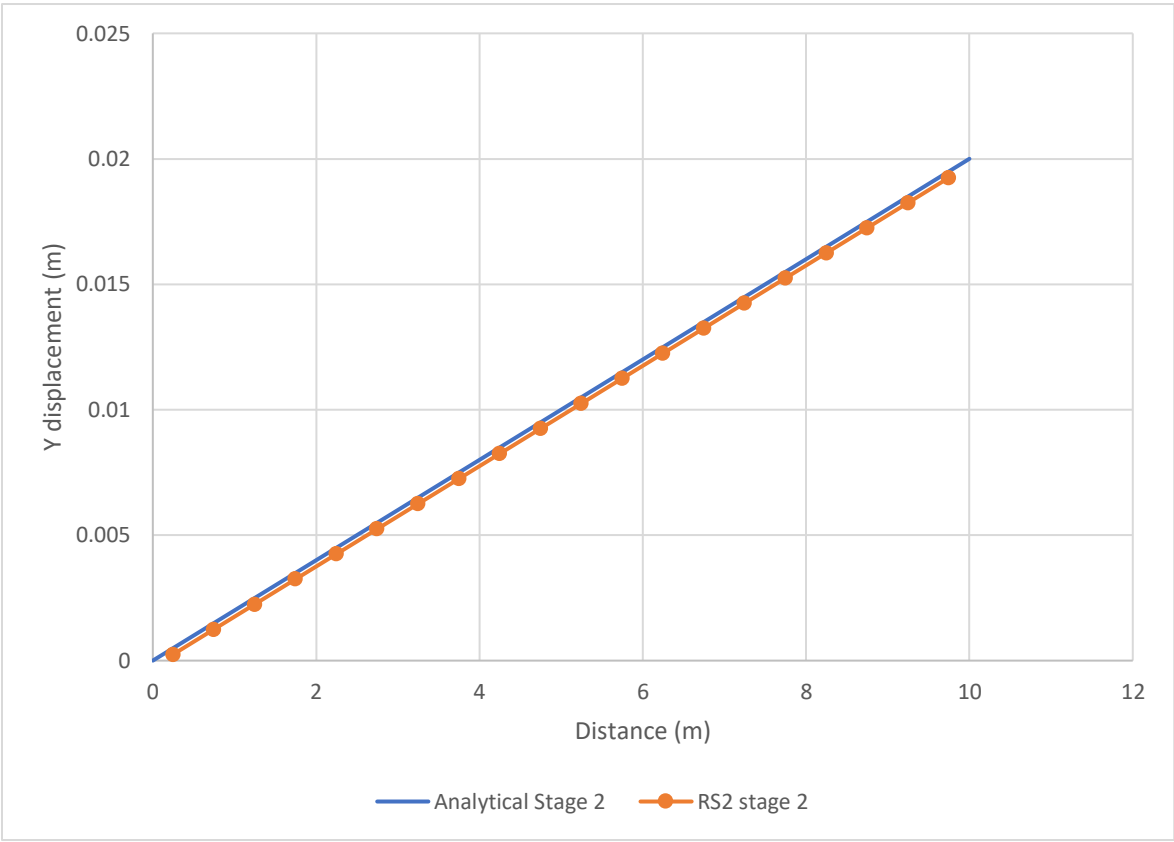


Figure 16.2: Vertical displacement in Y direction